Cellular/Molecular

Steering Neuronal Growth Cones by Shifting the Imbalance between Exocytosis and Endocytosis

Takuro Tojima,[1,2]* Rurika Itofusa,[1]* and Hiroyuki Kamiguchi[1]

[1]Laboratory for Neuronal Growth Mechanisms, RIKEN Brain Science Institute, Wako, Saitama 351-0198, Japan, and [2]PRESTO, Japan Science and Technology Agency, Kawaguchi, Saitama 332-0012, Japan

Extracellular molecular cues guide migrating growth cones along specific routes during development of axon tracts. Such processes rely on asymmetric elevation of cytosolic Ca^{2+} concentrations across the growth cone that mediates its attractive or repulsive turning toward or away from the side with Ca^{2+} elevation, respectively. Downstream of these Ca^{2+} signals, localized activation of membrane trafficking steers the growth cone bidirectionally, with endocytosis driving repulsion and exocytosis causing attraction. However, it remains unclear how Ca^{2+} can differentially regulate these opposite membrane-trafficking events. Here, we show that growth cone turning depends on localized imbalance between exocytosis and endocytosis and identify Ca^{2+}-dependent signaling pathways mediating such imbalance. In embryonic chicken dorsal root ganglion neurons, repulsive Ca^{2+} signals promote clathrin-mediated endocytosis through a 90 kDa splice variant of phosphatidylinositol-4-phosphate 5-kinase type-1γ (PIPKIγ90). In contrast, attractive Ca^{2+} signals facilitate exocytosis but suppress endocytosis via Ca^{2+}/calmodulin-dependent protein kinase II (CaMKII) and cyclin-dependent kinase 5 (Cdk5) that can inactivate PIPKIγ90. Blocking CaMKII or Cdk5 leads to balanced activation of both exocytosis and endocytosis that causes straight growth cone migration even in the presence of guidance signals, whereas experimentally perturbing the balance restores the growth cone's turning response. Remarkably, the direction of this resumed turning depends on relative activities of exocytosis and endocytosis, but not on the type of guidance signals. Our results suggest that navigating growth cones can be redirected by shifting the imbalance between exocytosis and endocytosis, highlighting the importance of membrane-trafficking imbalance for axon guidance and, possibly, for polarized cell migration in general.

Key words: **axon guidance; Ca^{2+}; endocytosis; exocytosis; growth cone**

Introduction

Axonal growth cones migrate along specific routes in the developing nervous system, changing direction in response to extracellular guidance cues (Tessier-Lavigne and Goodman, 1996). Most guidance cues instruct growth cone turning via asymmetric Ca^{2+} signals, with a higher Ca^{2+} concentration on the side of the growth cone facing the source of the cues, regardless of whether the cues are attractive or repulsive (Gomez and Zheng, 2006). In principle, the polarity of growth cone turning with respect to the Ca^{2+} localization is determined depending on the source of Ca^{2+} signals: primary Ca^{2+} signals through plasma membrane channels trigger repulsion away from the side with the signals, whereas primary Ca^{2+} signals together with secondary Ca^{2+} release from the endoplasmic reticulum (ER), for example, Ca^{2+}-induced Ca^{2+} release (CICR) through ryanodine receptors (RyRs), trigger attraction toward the side with the signals (Hong et al., 2000; Ooashi et al., 2005). Downstream of these attractive and repulsive Ca^{2+} signals, membrane trafficking acts as instructive machinery: locally activated exocytosis or endocytosis on one side of the growth cone drive attraction or repulsion, respectively (Tojima et al., 2011). It is also known that, through the Ca^{2+}/calmodulin-dependent protein phosphatase calcineurin, Ca^{2+} facilitates clathrin-mediated endocytosis for growth cone repulsion (Wen et al., 2004; Tojima et al., 2010). One hypothesis is that Ca^{2+} signals on one side of the growth cone create a localized imbalance between exocytosis and endocytosis, thereby steering the growth cone toward the side with more exocytosis or away from the side with more endocytosis. However, it remains largely unknown what signaling pathways link Ca^{2+} signals differentially with these opposite membrane-trafficking events to create such imbalance.

In presynaptic terminals, calcineurin and cyclin-dependent kinase 5 (Cdk5) counteractively regulate clathrin-mediated endocytosis after neurotransmitter release (Cousin and Robinson, 2001; Nguyen and Bibb, 2003; Tan et al., 2003; Tomizawa et al., 2003). In response to Ca^{2+} influx elicited by presynaptic excitation, calcineu-

Received Dec. 17, 2013; revised April 9, 2014; accepted April 15, 2014.

Author contributions: T.T., R.I., and H.K. designed research; T.T. and R.I. performed research; T.T. and R.I. analyzed data; T.T., R.I., and H.K. wrote the paper.

This work was supported by the Japan Science and Technology Agency PRESTO program (T.T.) and the Ministry of Education, Culture, Sports, Science and Technology of Japan (Grants-in-Aid for Scientific Research on Innovative Areas 23110005, Scientific Research C 24500393, and Young Scientists B 22700353 to T.T. and Scientific Research B 24300137 to H.K.). We thank A.T. Guy, A.V. Terashima, and C. Yokoyama for critical reading of this manuscript; J.H. Keen for providing the EGFP-clathrin construct; T. Fukuda for PIPKIγ cloning; T. Hida for advice on siRNA experiments; and the RIKEN BSI Research Resources Center for DNA sequencing.

The authors declare no competing financial interests.

*T.T. and R.I. contributed equally to this work.

Correspondence should be addressed to Hiroyuki Kamiguchi, Laboratory for Neuronal Growth Mechanisms, RIKEN Brain Science Institute, 2-1 Hirosawa, Wako, Saitama 351-0198, Japan. E-mail: kamiguchi@brain.riken.jp.

DOI:10.1523/JNEUROSCI.5261-13.2014

 0270-6474/14/347165-14$15.00/0

rin dephosphorylates and activates dephosphins, a group of clathrin-associated adaptor phosphoproteins including dynamin 1, amphiphysins, and a 90 kDa splice variant of phosphatidylinositol-4-phosphate 5-kinase type-1γ (PIPKIγ90), which then facilitate synaptic vesicle retrieval by clathrin-mediated endocytosis (Cousin and Robinson, 2001; Nakano-Kobayashi et al., 2007). This process can be antagonized by Cdk5-mediated phosphorylation of dephosphins (Nguyen and Bibb, 2003; Tomizawa et al., 2003). Because Ca^{2+}/calmodulin-dependent protein kinase II (CaMKII) interacts with and phosphorylates p35, an activation subunit of Cdk5, in a Ca^{2+}-dependent manner (Dhavan et al., 2002; Hosokawa et al., 2010), CaMKII could translate Ca^{2+} signals into Cdk5 activation, which inhibits clathrin-mediated endocytosis via dephosphin phosphorylation.

Here, we show that CaMKII and Cdk5 play a critical role in the generation of membrane-trafficking imbalance in growth cones. If this pathway is blocked, then attractive guidance signals facilitate both exocytosis and endocytosis and therefore fail to steer the growth cone. Experimental perturbation of this balanced activity in membrane trafficking restores the growth cone's turning response to guidance signals. Remarkably, the direction of this resumed turning depends on relative activities of exocytosis and endocytosis. Our results highlight the importance of membrane-trafficking imbalance for axon guidance.

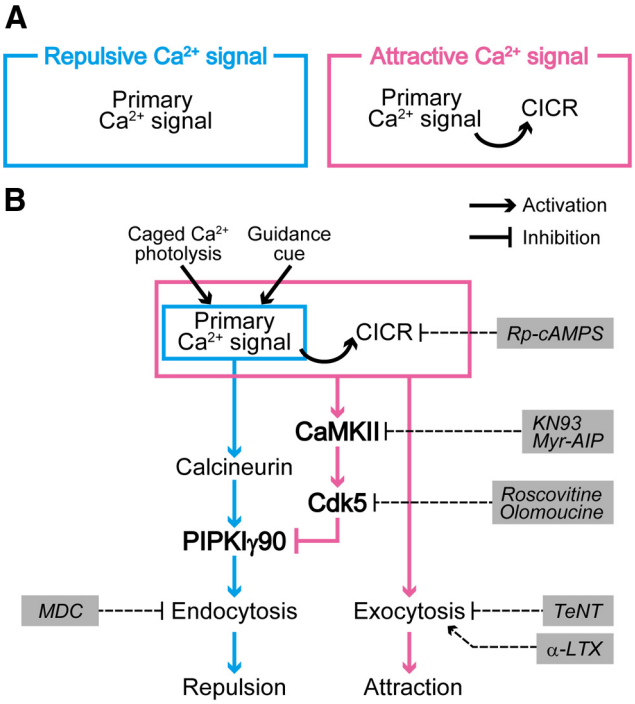

Figure 1. Schematic of proposed signaling pathways for Ca^{2+}-induced growth cone turning. ***A***, Components of attractive and repulsive Ca^{2+} signals. Our previous work (Ooashi et al., 2005) showed that repulsive Ca^{2+} signals (light blue rectangle) contain primary Ca^{2+} signals only, whereas attractive Ca^{2+} signals (pink rectangle) consist of primary Ca^{2+} signals and secondary CICR. ***B***, Hypothetical signaling pathways downstream of Ca^{2+} signals, in which light blue and pink arrows represent repulsive and attractive cascades, respectively. In the present study, primary Ca^{2+} signals were generated by repetitive photolysis of a caged Ca^{2+}, NP-EGTA, or by extracellular gradients of a physiological guidance cue, MAG. These primary Ca^{2+} signals can trigger CICR because RyRs are in the active state in our culture condition (Ooashi et al., 2005). To generate repulsive Ca^{2+} signals, we suppressed CICR by lowering cAMP level with the cAMP antagonist Rp-cAMPS. In this model, calcineurin and PIPKIγ90 act downstream of repulsive Ca^{2+} signals (light blue rectangle) to stimulate endocytosis for repulsion, whereas CaMKII and Cdk5 act downstream of attractive Ca^{2+} signals (pink rectangle) to suppress endocytosis for attraction. Together with CICR-stimulated exocytosis (Tojima et al., 2007), CaMKII and Cdk5 mediate an exocytosis–endocytosis imbalance on one side of the growth cone. Gray-shaded rectangles highlight pharmacological agents used in this study.

Materials and Methods

Cloning of chicken PIPKIγ. mRNA from embryonic day 9 (E9)–E10 chicken brain was isolated using the RNeasy Kit (QIAGEN). 3′-Rapid amplification of cDNA ends (3′-RACE) was performed with the 3′-Full RACE Core Set (Takara) using gene-specific primers (5′-CAGGCCT CGGATGAAGATGATGTGCCAGTCACAGAC-3′) and the supplied 3′ adaptor primer according to the manufacturer's instructions. We identified two PIPKIγ splice variants consisting of 639 and 667 aa, which correspond to mammalian PIPKIγ87 and PIPKIγ90, respectively (Ishihara et al., 1998; Funakoshi et al., 2011). These sequences were deposited in GenBank (accession numbers AB915769 and AB915768, respectively). The PCR products were run on agarose gels and individual DNA bands were excised, purified, and ligated into the pCR-BluntII-TOPO Vector (Invitrogen). Full-length PIPKIγ87 and PIPKIγ90 were amplified using the 5′ primer (5′-ATGGAGCTGGAGGTACCCGA-3′) and the 3′ primer (5′-CATCCCACTGGAACGGCTGCATCAAC-3′).

Plasmid constructs. Chicken PIPKIγ90 was subcloned into the XhoI-BamHI site of the pEGFP-N1 vector (Clontech). PIPKIγ90-D316A and PIPKIγ90-S649E were generated with the QuikChange Site-Directed Mutagenesis kit (Agilent Technologies). EGFP-Cdk5-WT and EGFP-Cdk5-D144N were gifts from L.-H. Tsai via Addgene (plasmid numbers 1346 and 1344, respectively). Venus-CaMKII-T286A and Venus-CaMKII-T286D were gifts from S. Vogel via Addgene (plasmid numbers 29430 and 29429, respectively). To generate mCherry-CAAX, the CAAX box of Ki-Ras corresponding to amino acid positions 169–188 (Kurokawa et al., 2001) was fused to the pmCherry-C1 vector (Clontech) using XhoI and BamHI.

Cell culture and transfection. Dorsal root ganglia (DRG) from E9–E10 chickens were treated with 0.05% trypsin-EGTA (Life Technologies) and dissociated by mechanical trituration. The dissociated neurons were plated on a glass-based dish. Unless otherwise noted, we used a dish coated with L1-Fc chimeric protein consisting of the extracellular domain of L1 and the Fc region of human IgG (Ooashi et al., 2005). The cultures were maintained in Leibovitz's L-15 medium (Invitrogen) supplemented with N2 (Invitrogen), 20 ng/ml nerve growth factor (Promega), and 750 μg/ml bovine serum albumin (Invitrogen) in a humidified atmosphere of 100% air at 37°C. For some experiments, dissociated neurons were transfected by electroporation (NEPA21; Nepagene) according to the manufacturer's instructions and cultured overnight before microscopic analyses. The transfected neurons were identified by the fluorescence of the transgene products.

RNA interference. Small interfering RNA (siRNA) sequences for chicken PIPKIγ were designed with the BLOCK-iT RNAi Designer program (Invitrogen) and purchased from Invitrogen. The targeting sequences were 5′-GGTACTTCCGAGAACTCTT-3′ and 5′-GCACTA CCGTAGCTACCTA-3′ for PIPKIγ siRNA #1 and #2, respectively. The targeting sequence for control siRNA was 5′-TCTTCCCCCAAGAAA GATA-3′, which does not exist in the chicken genome (Endo et al., 2007). These siRNAs were introduced into DRG neurons by trituration loading as described previously (Nishimura et al., 2003). In brief, trypsinized neurons were triturated using a P20 Pipetman (Gilson) for ~140 strokes in 20 μl of L-15 medium containing 50 μM siRNA and 50 μM Alexa Fluor 594-conjugated dextran (molecular weight 10,000; Invitrogen). The dissociated neurons were cultured overnight before immunoblotting or microscopic analyses. Neurons emitting Alexa Fluor 594 fluorescence were included in microscopic analyses.

Immunoblotting. DRG neurons cultured on L1 substrate for 24 h were harvested in lysis buffer (20 mM HEPES, pH 7.4, 5 mM EDTA, 120 mM NaCl, 10% glycerol, 1% Triton X-100) supplemented with a protease inhibitor mixture (Roche). Samples for protein phosphorylation analyses were also treated with 0.04 U/μl lambda protein phosphatase (λ-PPase; BioAcademia) for 30 min at 30°C. All samples were suspended in sample preparation buffer (final concentration: 62.5 mM Tris-HCl, pH 6.8, 2% SDS, 5% sucrose, 5% 2-mercaptoethanol, 0.002% bromophenol blue), subjected to SDS-PAGE, and then trans-

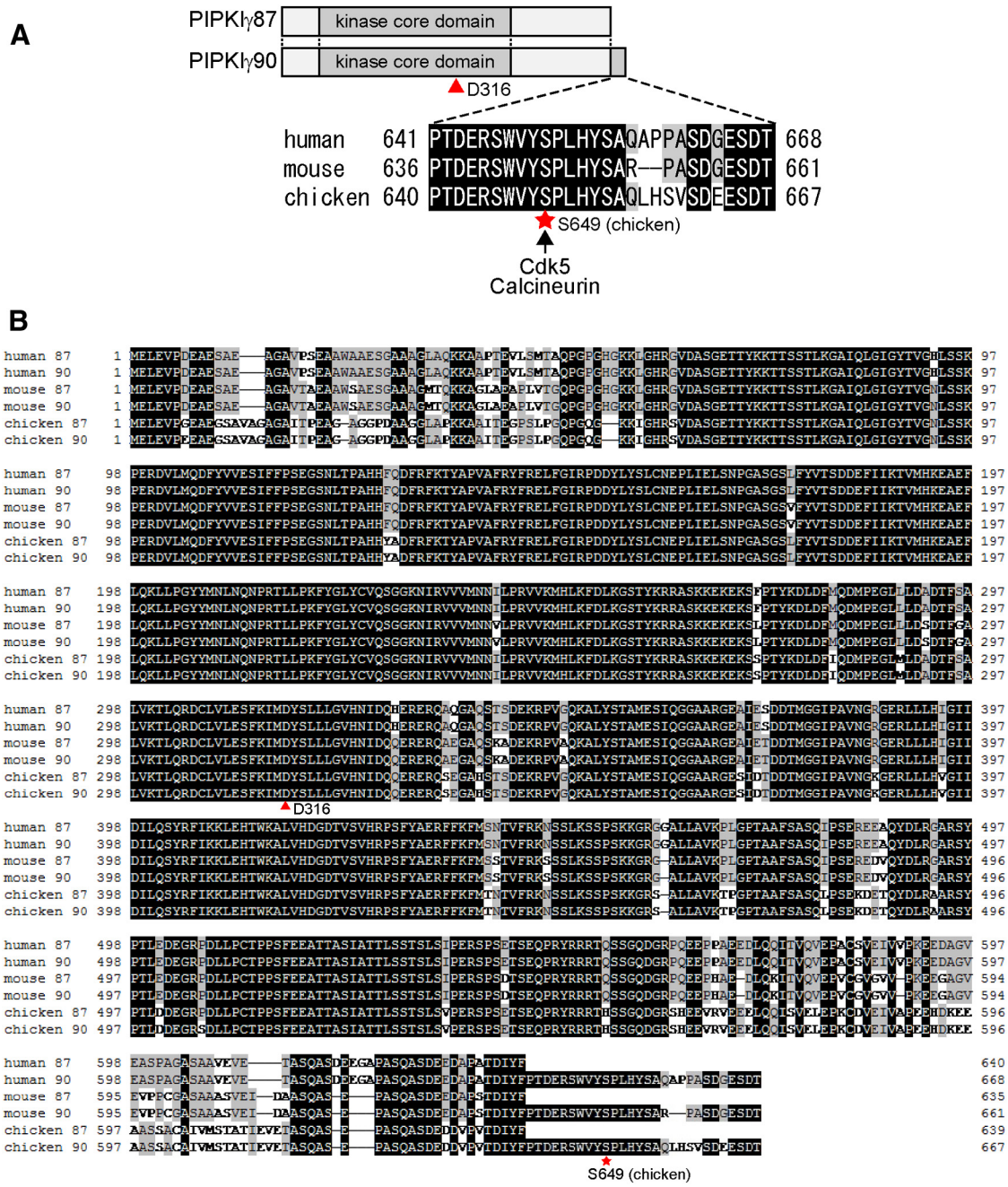

Figure 2. Alignment of amino acid sequences of PIPKIγ. ***A***, Schematic representation of the PIPKIγ splice variants PIPKIγ87 and PIPKIγ90. We cloned chicken PIPKIγ87 encoding 639 aa and PIPKIγ90 containing additional 28 aa at the C terminus (667 aa in total). The amino acid sequence of the C-terminal stretch of chicken PIPKIγ90 was compared with that of human and mouse PIPKIγ90. This C-terminal region is highly conserved among these species and contains a serine residue that can be phosphorylated/dephosphorylated by Cdk5/calcineurin (S649 in chicken; red star). We made a phosphomimetic mutant (S649 to E substitution) and a kinase-dead mutant (D316 to A substitution; red arrowhead) of chicken PIPKIγ90. ***B***, Full amino acid sequences of PIPKIγ87 and PIPKIγ90 in human, mouse, and chicken. Black boxes represent completely conserved sequences. Gray boxes represent sequence conservation >60%. Dashes indicate the absence of corresponding amino acids.

ferred to a polyvinylidene difluoride membrane (Millipore). The membrane was treated with a blocking solution (Blocking One; Nacalai Tesque) for 60 min at room temperature and then incubated with rabbit anti-mouse PIPKIγ monoclonal antibody (1:10,000; catalog #ab109192; Abcam) or mouse anti-β-tubulin monoclonal antibody (1:10,000; catalog #MAB3408; Millipore) overnight at 4°C. After washing, the membrane was incubated with HRP-conjugated secondary antibody against rabbit or mouse IgG (1:10,000; GE Healthcare). The blots were then visualized with Luminata Forte Western HRP substrate (Millipore) on an x-ray film, followed by intensity quantification using ImageJ version 1.47 software.

Immunocytochemistry. DRG neurons cultured on L1 substrate were fixed in fixation buffer (80 mM Na-PIPES, pH 6.9, 1 mM $MgCl_2$, 1 mM EGTA, 1 mM GTP, 3% sucrose, 0.1% glutaraldehyde, 4% formaldehyde) for 30 min at 37°C, permeabilized with 0.1% Triton X-100 for 60 min, and then incubated with rabbit anti-mouse PIPKIγ monoclonal antibody (1:500) overnight at 4°C. Primary antibody binding was visualized with Alexa Fluor 488-conjugated goat anti-rabbit IgG (1:200; Invitrogen). Fluorescence and differential interference contrast (DIC) images were taken using an inverted microscope (IX81; Olympus) equipped with a 100× objective [UPLSAPO, oil, numerical aperture (NA) 1.40; Olympus] and a charge coupled device

(CCD) camera (ORCA-AG with binning set at 1 × 1; Hamamatsu Photonics).

Pharmacological agents. Unless otherwise noted, the following reagents were applied to some cultures at least 30 min before the experiments: 20 μM Rp-cAMPS (Calbiochem), 30 nM KN93 (Sigma), 1 μM myristoylated autocamtide-2-inhibitory peptide (myr-AIP; Enzo Life Science), 30 nM roscovitine (Enzo Life Science), 3 μM olomoucine (Calbiochem), 5 nM tetanus neurotoxin (TeNT; List), 1 μM monodansylcadaverine (MDC; Sigma), and 100 μM ryanodine (Latoxan). Neurons were loaded with 1 μM an acetoxymethyl ester derivative of 1,2-bis(*o*-aminophenoxy) ethane-*N*,*N*,*N*′,*N*′-tetraacetic acid (BAPTA-AM; Invitrogen) as described previously (Ooashi et al., 2005).

Total internal reflection fluorescence microscopy combined with UV photolysis. To determine the effect of Ca^{2+} signals on clathrin-coated pit (CCP) formation, neurons expressing EGFP-clathrin (a gift from J.H. Keen; Gaidarov et al., 1999) or mCherry-clathrin (Tojima et al., 2010) were loaded with 2 μM an acetoxymethyl ester derivative of *o*-nitrophenyl EGTA (NP-EGTA-AM; Invitrogen) in the presence of 0.0025% Cremophor EL (Nacalai Tesque) for 30 min. We used a custom-built microscope (Tojima et al., 2010) comprised of an upright UV photolysis unit (Olympus) and an inverted microscope (IX81; Olympus) equipped with an illumination system (IX2-RFAEVA-2; Olympus) for total internal reflection fluorescence microscopy (TIRFM) and a 100× objective (UApoN TIRFM, oil, NA 1.49; Olympus). EGFP or mCherry immediately adjacent to the cover glass–cell interface was excited with evanescent waves of a 488 nm solid-state laser (Melles Griot) or a 561 nm solid-state laser (LASOS Lasertechnik), and its emission was collected through a band-pass filter (FF01-514/30; Semrock) or a long-pass filter (BA610IF; Olympus), respectively. Images were acquired with MetaMorph version 7.7 software (Molecular Devices) and a CCD camera (ORCA-AG with binning set at 2 × 2) every 3 s before and after the onset of repetitive UV irradiation. NP-EGTA was photolyzed by repetitive UV irradiation for a duration of 100 ms every 3 s in the area that covered the central domain periphery to the leading edge on one side of the growth cone (~10 μm in diameter). The border between the central and peripheral domain was determined on a DIC image of the growth cone (Tojima et al., 2007). To assess the asymmetry in endocytosis, the UV-irradiated area and the corresponding area on the opposite side of a growth cone were defined as the near and far regions of interest (ROIs), respectively. Far ROIs were positioned by an observer blind to the experimental conditions. The number of newly formed clathrin puncta within a ROI was normalized by the growth cone area covered by that ROI.

TIRFM combined with extracellular myelin-associated glycoprotein gradient application. As described previously (Tojima et al., 2010), myelin-associated glycoprotein (MAG) gradients were applied to a growth cone cultured on laminin substrate (a dish coated with ~50 ng/cm^2 laminin; Invitrogen) through a micropipette containing MAG (150 μg/ml; R&D Systems) that was positioned 50 μm from the growth cone with 90° angle with respect to the original direction of axon elongation. A graded distribution of the reagent was formed across the growth cone within 1 min after the onset of pulsate positive pressure in the pipette (amplitude, 4 psi; pulse width, 20 ms; interpulse interval, 500 ms; Akiyama et al., 2009). To monitor clathrin-mediated endocytosis, growth cones expressing EGFP-clathrin were observed under the inverted TIRFM system equipped with a 100× objective (PlanApo TIRFM, oil, NA 1.45; Olympus). Images were acquired every 3 s before and after the onset of MAG application. To assess the asymmetry in endocytosis, two circular ROIs (~10 μm in diameter) were positioned on the near and far side of the growth cone by an observer blind to the experimental conditions. The number of newly formed clathrin puncta within a ROI was normalized by the growth cone area covered by that ROI.

To monitor vesicle-associated membrane protein 2 (VAMP2)-mediated exocytosis, growth cones expressing pHVenus-VAMP2 (Tojima et al., 2007) and mCherry-CAAX were observed under the inverted TIRFM system. pHVenus and mCherry were excited simultaneously with 488 and 561 nm laser, respectively, and their emissions were split by a dichroic mirror (565dcxr; Chroma) equipped in an emission splitter (DV2; Photometrics). The split emissions were collected through band-pass filters (D520/30 for pHVenus and D630/50 for mCherry; Chroma) and acquired simultaneously with a CCD camera (Evolve with binning set at 4 × 4; Photometrics) every 3 s before and after the onset of MAG application. To assess the asymmetry in exocytosis, fluorescence intensities (F) of pHVenus and of mCherry were averaged within near and far ROIs defined as described previously (Akiyama et al., 2009). F/F_0 was

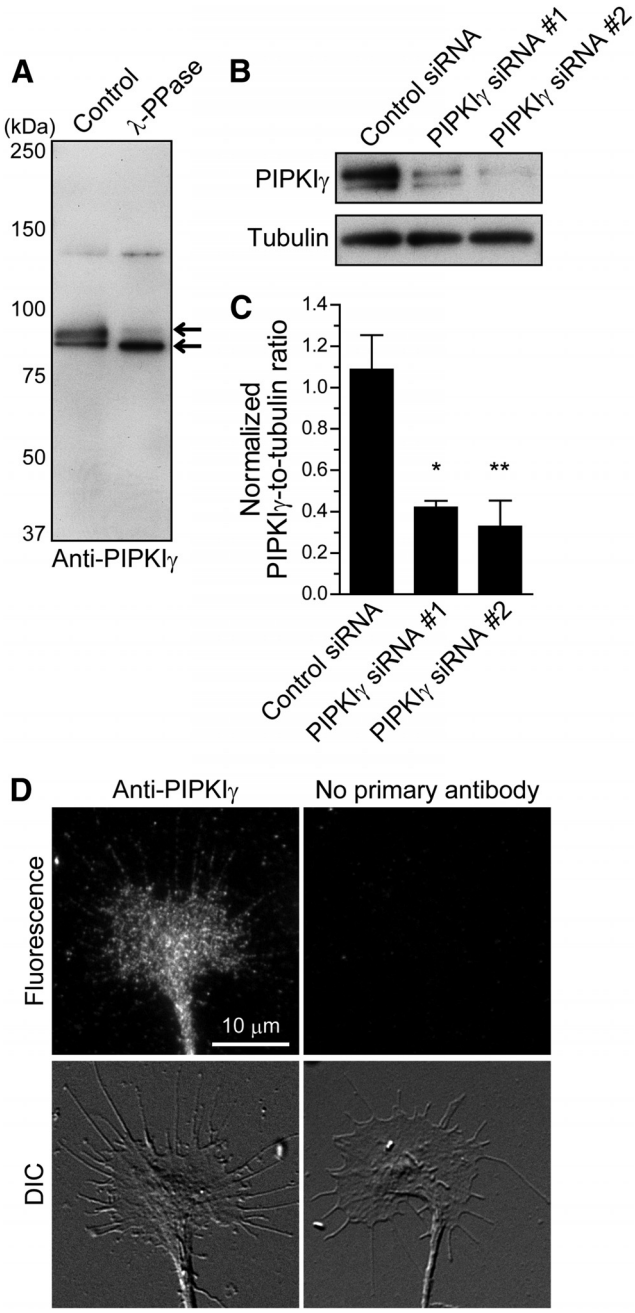

Figure 3. Embryonic DRG neurons express PIPKIγ. ***A***, PIPKIγ immunoblotting of cultured embryonic chicken DRG neuron lysates showing two bands at ~90 kDa. Their differential sensitivities to λ-PPase treatment suggest the presence of phosphorylated (top arrow) and unphosphorylated (bottom arrow) forms of PIPKIγ. Shown is a representative of three independent experiments. ***B***, PIPKIγ immunoblots showing the effect of siRNAs (control siRNA, PIPKIγ siRNA#1 and #2) with tubulin immunoblots as a loading control. ***C***, Quantification of PIPKIγ knock-down. PIPKIγ-to-tubulin ratios of immunoblot intensities after siRNA treatment were normalized to those without siRNA. $*p < 0.05$, $**p < 0.01$ versus control siRNA, Dunnett's multiple-comparison test ($n = 3$ independent experiments). ***D***, PIPKIγ immunofluorescence and corresponding DIC images of a DRG growth cone (left) and images of no primary antibody control (right). Scale bar, 10 μm.

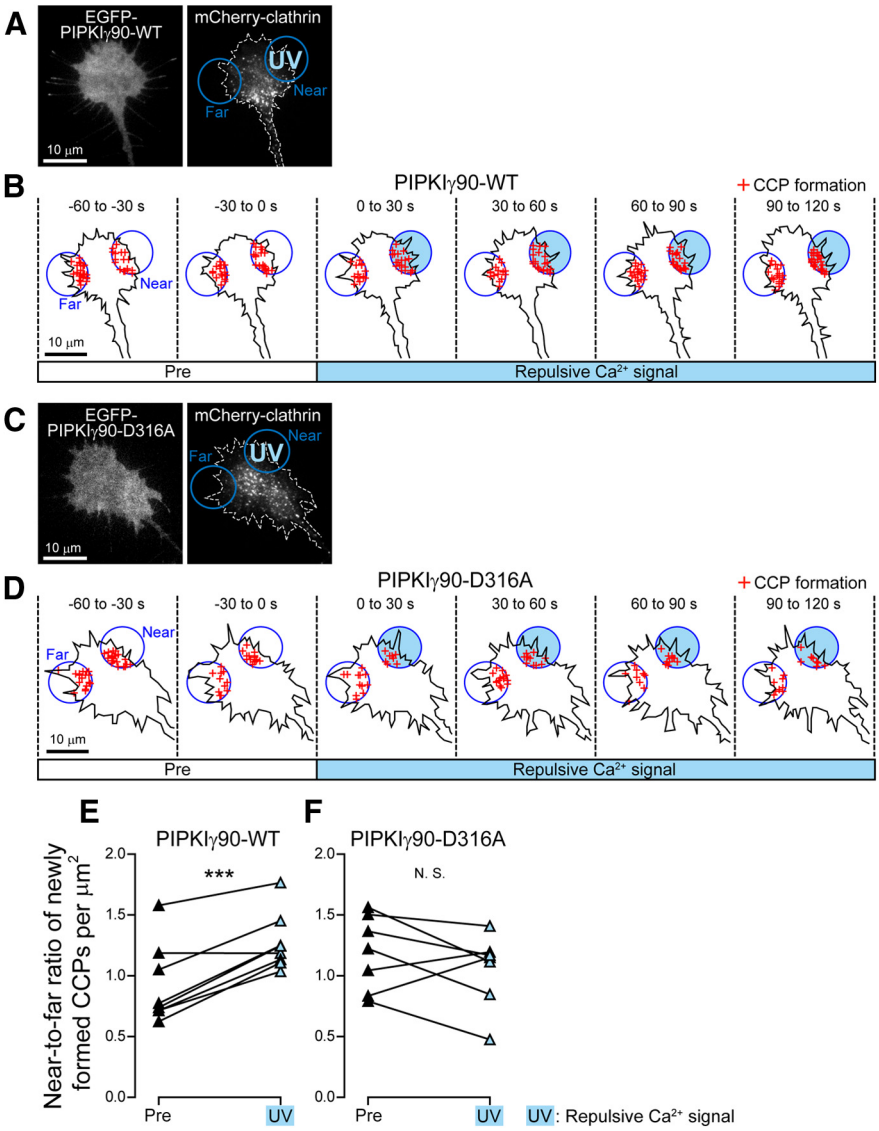

Figure 4. PIPKIγ90 mediates asymmetric endocytosis induced by repulsive Ca^{2+} signals. ***A–D***, Effects of wild-type (WT) PIPKIγ90 (***A***, ***B***) or its kinase-dead mutant D316A (***C***, ***D***) on asymmetric endocytosis induced by repulsive Ca^{2+} signals. ***A***, ***C***, TIRFM images of single growth cones coexpressing EGFP-PIPKIγ90 (left) and mCherry-clathrin (right). NP-EGTA was photolyzed by repetitive UV light (3 s interval) in the presence of Rp-cAMPS to generate repulsive Ca^{2+} signals. The UV-irradiated area and the corresponding area on the opposite side were used as near and far ROIs, respectively (blue circles). Scale bars, 10 μm. ***B*** and ***D*** show schematic representations of the growth cone in ***A*** and ***C***, respectively. TIRFM images of mCherry-clathrin were acquired every 3 s before (pre) and after the onset (time 0 s) of repulsive Ca^{2+} signals. Each red cross marks the position of a newly formed CCP within the ROIs during the indicated 30 s periods. Scale bars, 10 μm. ***E***, ***F***, Near-to-far ratios of CCP formation in growth cones expressing EGFP-PIPKIγ90-WT (***E***) or EGFP-PIPKIγ90-D316A (***F***). The *y*-axis indicates the number of newly formed CCPs per unit area within near ROI divided by that within far ROI, before (pre; −120 to 0 s) and after (UV; 0 to 120 s) the onset of repulsive Ca^{2+} signals. Each line represents Ca^{2+}-induced change in a single growth cone. ***$p < 0.001$; N.S., not significant, paired *t* test.

calculated individually for pHVenus and mCherry, where F_0 was the mean of 40 consecutive F values taken from −120 to −3 s (i.e., before the onset of MAG application). The F/F_0 values for pHVenus and mCherry were designated as $R_{pHVenus}$ and $R_{mCherry}$, respectively. The $R_{pHVenus}/R_{mCherry}$ values, designated as R', were determined for near ROI (R'_{near}) and for far ROI (R'_{far}). Changes in the asymmetry in exocytosis were expressed as $\Delta(R'_{near}/R'_{far})$, where $\Delta(R'_{near}/R'_{far}) = R'_{near}/R'_{far} - 1$.

Growth-cone-turning assays. Growth cone turning induced by focal laser-induced photolysis of NP-EGTA was performed on L1 substrate as described previously (Ooashi et al., 2005). Growth cone turning induced by extracellular gradients of MAG (150 μg/ml in pipette), MDC (100 μM in pipette), and α-latrotoxin (α-LTX, 10 nM in pipette; Sigma) was performed on laminin substrate as described previously (Akiyama et al., 2009).

Imaging of photolysis-induced Ca^{2+} signals. Attractive Ca^{2+} signals generated by focal laser-induced photolysis in a growth cone were visualized by simultaneous and ratiometric imaging of two fluorescent Ca^{2+} indicators, Oregon Green BAPTA-1 (OGB-1) and Fura Red (FR) as described previously (Tojima et al., 2009). Cultured neurons were loaded simultaneously with 2 μM OGB-1-AM (Invitrogen), 2 μM FR-AM (Invitrogen), and 2 μM NP-EGTA-AM in the presence of 0.0025% Cremophor EL for 30 min, followed by a wash. The neurons were postincubated for >30 min and then observed under an inverted microscope (IX71; Olympus) equipped with a 100× objective (UPLSAPO) and a CCD camera (ORCA-ER with binning set at 8 × 8; Hamamatsu Photonics). OGB-1 and FR were excited simultaneously with a 75 W xenon lamp using an excitation filter (460–495BP; Olympus) and a dichroic mirror (72100bs; Chroma). The OGB-1 and FR emissions were split by a dichroic mirror (DM590LP; Hamamatsu Photonics) equipped in an emission splitter (W-view; Hamamatsu Photonics). The split OGB-1 and FR emissions were collected through a band-pass filter (535AF45; Omega) and a long-pass filter (BA610IF; Olympus), respectively. The images of OGB-1 and FR were simultaneously acquired every 22.1 ms at an exposure of 10.2 ms. For photolysis of NP-EGTA, five laser pulses (a pulse width of 5 ns) were shot onto a growth cone at 442 ms intervals, which corresponded to one laser pulse per 20 flames of Ca^{2+} imaging. The laser-shot timing was controlled by AquaCosmos version 2.6 software (Hamamatsu Photonics) and an electronic stimulator (Nihon Koden) such that a camera exposure was initiated 0.9 ms after the laser shot. This interval was sufficiently long to prevent laser-induced artifacts from affecting Ca^{2+} imaging (Ooashi et al., 2005). For quantitative analyses, a ROI (ϕ2.6 μm circular zone) was positioned within a growth cone such that the ROI was centered by the photolysis site. After background subtraction, F values for OGB-1 and FR were averaged within the ROIs. Relative fluorescence over the basal fluorescence (F/F_0) was calculated individually for OGB-1 and FR channels. Here, F_0 is a mean of nine consecutive F values taken from 0 to 176.6 ms (before the first laser shot). The F/F_0 values for OGB-1 and FR channels were designated as $R_{OGB\text{-}1}$ and R_{FR}, respectively. Changes in cytosolic Ca^{2+} levels were expressed as $\Delta(R_{OGB\text{-}1}/R_{FR})$, where $\Delta(R_{OGB\text{-}1}/R_{FR}) = R_{OGB\text{-}1}/R_{FR} - 1$. Positive and negative $\Delta(R_{OGB\text{-}1}/R_{FR})$ values indicate that Ca^{2+} levels increase and decrease, respectively, with respect to the basal Ca^{2+} level, where the basal Ca^{2+} level is the mean of nine frames taken from 0 to 176.6 ms (before the first laser shot). The effect of drugs on photolysis-induced Ca^{2+} elevations was evaluated by comparing the amplitude of $\Delta(R_{OGB\text{-}1}/R_{FR})$ spikes before and after 5 min treatment with the drugs in the same growth cone. The drug-induced changes in the amplitude of $\Delta(R_{OGB\text{-}1}/R_{FR})$ spikes were expressed as $\Delta R'_{after}/\Delta R'_{before}$, where $\Delta R'_{before}$ and $\Delta R'_{after}$ indicate the mean of five peak $\Delta(R_{OGB\text{-}1}/R_{FR})$ values induced by five laser pulses before and after the drug treatment, respectively.

Statistics. Data are expressed as the mean ± SEM. Statistical analyses were performed using Prism version 5.04 software (GraphPad). $p < 0.05$ was considered statistically significant.

Results

Generation of attractive or repulsive Ca^{2+} signals

We used a caged Ca^{2+} compound, NP-EGTA, to generate Ca^{2+} signals on one side of the growth cone of an embryonic chicken DRG neuron. We showed previously that one primary distinction between attractive and repulsive Ca^{2+} signals is the occurrence of CICR through RyRs that is regulated by extracellular substrates via cAMP signaling (Ooashi et al., 2005; Fig. 1). In growth cones cultured on the cell adhesion molecule L1, Ca^{2+} liberated from NP-EGTA upon photolysis (primary Ca^{2+} signals) triggers secondary CICR through RyRs, which causes growth cone attraction. In the presence of the cAMP antagonist Rp-cAMPS that inactivate RyRs, however, the photolysis-induced primary Ca^{2+} signals are not accompanied by CICR and therefore trigger growth cone repulsion. Such CICR-dependent switching mechanism also operates in growth cone guidance induced by physiological cues (Hong et al., 2000). In our experiments, attractive or repulsive Ca^{2+} signals were generated by photolyzing NP-EGTA in neurons on L1 substrate in the absence or presence of Rp-cAMPS, respectively, as described previously (Tojima et al., 2010).

PIPKIγ90 mediates asymmetric clathrin-mediated endocytosis induced by repulsive Ca^{2+} signals

We reported previously that repulsive Ca^{2+} signals evoke asymmetric clathrin-mediated endocytosis for growth cone repulsion in a calcineurin-dependent manner (Tojima et al., 2010). Therefore, here, we investigated whether PIPKIγ90, a dephosphin, acts downstream of repulsive Ca^{2+} signals to regulate clathrin-mediated endocytosis in growth cones (Figs. 2, 3, 4). PIPKI catalyzes the production of the membrane phospholipid phosphatidylinositol (4,5)-bisphosphate (PIP_2), which plays a key role in recruiting endocytic machinery components to the plasma membrane (Loijens and Anderson, 1996; Sasaki et al., 2009; Funakoshi et al., 2011). Of three PIPKI isozymes (α, β, and γ) identified in rodents and humans, PIPKIγ is predominantly expressed in the brain (Wenk et al., 2001) and has at least two splicing variants, PIPKIγ87 and PIPKIγ90. PIPKIγ90 has a C-terminal stretch composed of ~30 aa (Fig. 2; Di Paolo et al., 2002; Ling et al., 2002; Sasaki et al., 2009; Funakoshi et al., 2011) that contains a phosphorylation/dephosphorylation site for Cdk5/calcineurin (Lee et al., 2005; Nakano-Kobayashi et al., 2007). At presynaptic terminals, the dephosphorylated PIPKIγ90 becomes enzymatically active and produces PIP_2 to initiate clathrin-mediated synaptic vesicle endocytosis (Nakano-Kobayashi et al., 2007).

We cloned chicken PIPKIγ from embryonic brain and identified two splice variants consisting of 639 and 667 aa, which are 84% identical to human PIPKIγ87 and PIPKIγ90, respectively (Fig. 2). Importantly, the C-terminal stretch of PIPKIγ90 has a highly conserved sequence among mammals and chicken and carries a Cdk5 phosphorylation site. We examined endogenous PIPKIγ expression in cultured embryonic chicken DRG neurons by immunoblot and immunocytochemical analyses (Fig. 3). An antibody raised against mouse full-length PIPKIγ detected two immunoblots at ~90 kDa (Fig. 3*A*, left). Intensities of these blots decreased significantly after the introduction of siRNAs targeted against chicken PIPKIγ (Fig. 3*B*, *C*), indicating that this antibody can recognize chicken PIPKIγ. Treatment with λ-PPase attenuated the upper blot and augmented the lower blot (Fig. 3*A*, right), strongly suggesting that DRG neurons express the phosphorylatable isoform PIPKIγ90. In addition, immunocytochemistry showed PIPKIγ expression throughout the growth cone of cultured DRG neurons (Fig. 3*D*).

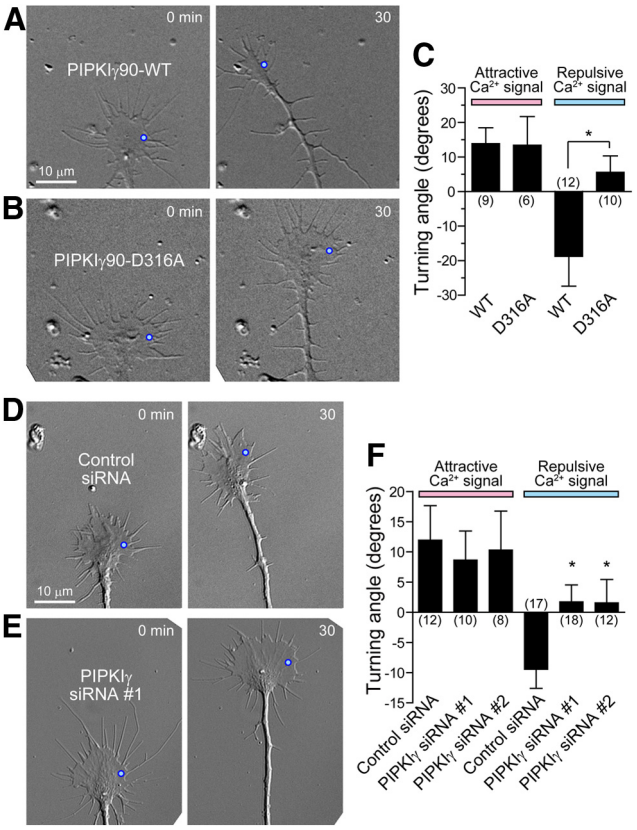

Figure 5. PIPKIγ90 mediates Ca^{2+}-induced growth cone repulsion. ***A***, ***B***, Time-lapse DIC images of a growth cone expressing EGFP tagged to wild-type (WT; ***A***) or kinase-dead mutant (D316A; ***B***) of PIPKIγ90. Repulsive Ca^{2+} signals were generated by laser photolysis of NP-EGTA at light blue spots. Time in minutes after the onset of repetitive laser irradiation (3 s interval) is shown. Scale bar, 10 μm. ***C***, Ca^{2+}-induced turning of growth cones expressing EGFP-PIPKIγ90-WT or EGFP-PIPKIγ90-D316A. Attractive (pink) or repulsive (light blue) Ca^{2+} signals were generated on one side of the growth cones. Positive and negative values expressed as mean ± SEM indicate attractive and repulsive turning angles, respectively. Numbers in parentheses indicate the number of growth cones examined. *$p < 0.05$, unpaired *t* test. ***D***, ***E***, Time-lapse DIC images of a growth cone containing control siRNA (***D***) or PIPKIγ siRNA #1 (***E***). Repulsive Ca^{2+} signals were generated by laser photolysis of NP-EGTA at light blue spots. Scale bar, 10 μm. ***F***, Ca^{2+}-induced turning of growth cones containing control siRNA, PIPKIγ siRNA #1 or #2. *$p < 0.05$ versus control siRNA, Dunnett's multiple-comparison test.

To determine the role of PIPKIγ90 kinase activity in growth cones, we transfected DRG neurons with an expression plasmid encoding EGFP-tagged kinase-dead mutant of chicken PIPKIγ90, in which Asp was replaced with Ala at position 316 (PIPKIγ90-D316A; Unoki et al., 2012), or EGFP-tagged wild-type chicken PIPKIγ90 (PIPKIγ90-WT) as a control (Fig. 4). The neurons were cotransfected with mCherry-tagged clathrin light chain (Gaidarov et al., 1999) to analyze the spatiotemporal dynamics of clathrin in growth cones by TIRFM. This method has been used extensively to visualize the formation of CCPs and clathrin-coated vesicles, both processes involved in clathrin-mediated endocytosis (Merrifield et al., 2002; Rappoport and Simon, 2003; Tojima et al., 2010). Using a custom-built microscope comprised of an upright UV-photolysis unit and an inverted TIRFM system (Tojima et al., 2010), we evoked repulsive Ca^{2+} signals by repetitive photolysis of NP-EGTA on one side of

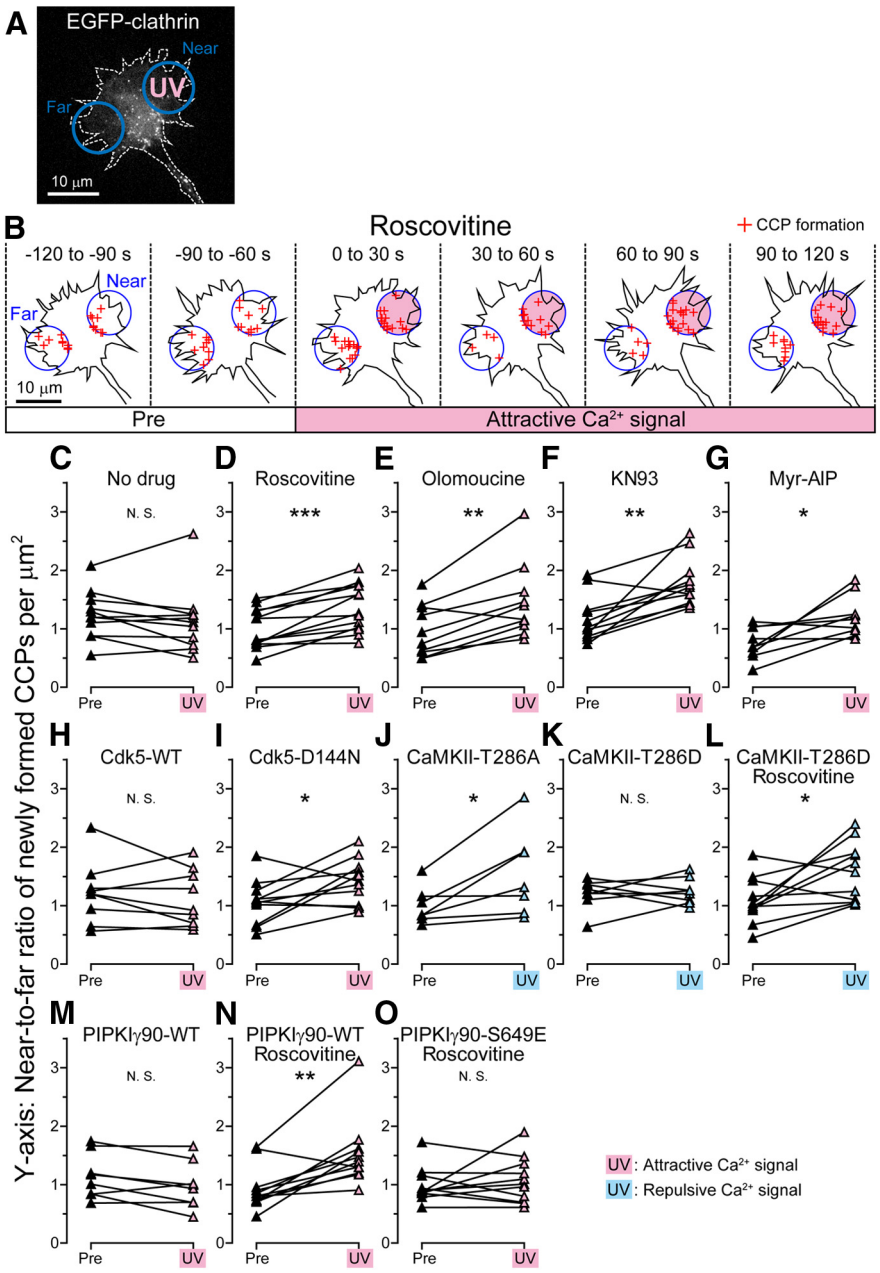

Figure 6. Attractive Ca^{2+} signals suppress endocytosis via CaMKII and Cdk5. ***A***, TIRFM image of EGFP-clathrin in a growth cone treated with roscovitine. NP-EGTA was photolyzed by repetitive UV light (3 s interval) to generate attractive Ca^{2+} signals. The UV-irradiated area and the corresponding area on the opposite side were used as near and far ROIs, respectively (blue circles). Scale bar, 10 μm. ***B***, Schematic representation of the growth cone shown in ***A***. TIRFM images of EGFP-clathrin were acquired every 3 s before (pre) and after the onset (time 0 s) of attractive Ca^{2+} signals. Each red cross marks the position of a newly formed CCP within the ROIs during the indicated 30 s periods. Scale bar, 10 μm. ***C–O***, Near-to-far ratios of CCP formation. Growth cones expressing EGFP-clathrin (***C–G***) or mCherry-clathrin (***H–O***) were analyzed. The *y*-axis indicates the number of newly formed CCPs per unit area within near ROI divided by that within far ROI, before (pre; −120 to 0 s) and after (UV; 0 to 120 s) the onset of repetitive photolysis that generated attractive (pink; ***C–I***, ***M–O***) or repulsive (light blue; ***J–L***) Ca^{2+} signals. Each line represents a photolysis-induced change in a single growth cone. Ca^{2+}-induced asymmetry in CCP formation was assessed in the absence (no drug; ***C***) or presence of roscovitine (***D***, ***L***, ***N***, ***O***), olomoucine (***E***), KN93 (***F***), or myr-AIP (***G***). In addition, the asymmetry was assessed in growth cones that had been transfected with EGFP-tagged wild-type (WT; ***H***) and the dominant-negative form (D144N; ***I***) of Cdk5, Venus-tagged phosphodeficient (T286A; ***J***), and phosphomimetic (T286D; ***K***, ***L***) mutants of CaMKII or EGFP-tagged wild-type (WT; ***M***, ***N***) and phosphomimetic mutant (S649E; ***O***) of PIPKIγ90. $*p < 0.05$, $**p < 0.01$, $***p < 0.001$; N.S., not significant, paired *t* test.

a growth cone and compared endocytic activity in the UV-irradiated area (near) against that in the corresponding area on the opposite side (far). We counted the number of newly formed clathrin puncta as a measure of CCP formation. In response to repulsive Ca^{2+} signals, growth cones expressing PIPKIγ90-WT showed asymmetric CCP formation with higher endocytic activity in the near side (Fig. 4*A*,*B*,*E*). Conversely, repulsive Ca^{2+} signals failed to evoke asymmetric CCP formation in growth cones expressing PIPKIγ90-D316A (Fig. 4*C*,*D*,*F*). These results suggest that the kinase activity of PIPKIγ90 mediates the facilitation of clathrin-mediated endocytosis downstream of repulsive Ca^{2+} signals.

PIPKIγ90 mediates Ca^{2+}-induced growth cone repulsion

We next investigated the involvement of PIPKIγ90 in Ca^{2+}-induced growth cone turning (Fig. 5). Bidirectional turning was triggered by repetitive photolysis of NP-EGTA on one side of a growth cone (Ooashi et al., 2005). Repulsive Ca^{2+} signals caused no detectable turning of growth cones expressing EGFP-tagged PIPKIγ90-D316A, but elicited repulsive turning of growth cones expressing EGFP-tagged PIPKIγ90-WT (Fig. 5*A*–*C*). Conversely, attractive Ca^{2+} signals induced attractive turning of growth cones expressing either form of PIPKIγ90 (Fig. 5*C*). We further investigated the role of endogenous PIPKIγ using an siRNA knock-down approach (Fig. 5*D*–*F*). Two different siRNAs directed against chicken PIPKIγ (#1 and #2; Fig. 3*B*,*C*) abolished Ca^{2+}-induced growth cone repulsion but not attraction (Fig. 5*E*,*F*), whereas control siRNA had no detectable effect on either growth cone attraction or repulsion (Fig. 5*D*,*F*). These results indicate that PIPKIγ90 is necessary for Ca^{2+}-induced growth cone repulsion but not attraction.

Attractive Ca^{2+} signals suppress clathrin-mediated endocytosis via CaMKII and Cdk5

In presynaptic terminals, the endocytosis-promoting activity of PIPKIγ90 is blocked by Cdk5-mediated phosphorylation of PIPKIγ90 (Nakano-Kobayashi et al., 2007). We therefore tested whether Cdk5 negatively regulates clathrin-mediated endocytosis downstream of attractive Ca^{2+} signals using TIRFM of fluorescently labeled clathrin in growth cones treated with pharmacological and genetic inhibitors (Fig. 6). In the absence of inhibitors (no drug), attractive Ca^{2+} signals did not cause asymmetric CCP formation across the growth cone (Fig. 6*C*) even though the signals contained a repulsive component: primary Ca^{2+} liberated from NP-EGTA (Fig. 1). This result is consistent with our previous finding (Tojima et al., 2010). However, inhibition of Cdk5 with roscovitine or olomoucine allowed growth cones to have asymmetric CCP formation in response to attractive Ca^{2+} signals (Fig. 6*A*,*B*,*D*,*E*). In addition, asymmetric

CCP formation was induced by attractive Ca^{2+} signals in growth cones expressing EGFP-tagged kinase-dead mutant of Cdk5, in which Asp was replaced with Asn at 144 (Cdk5-D144N; Nikolic et al., 1996), whereas no asymmetry was detected in control growth cones expressing EGFP-tagged wild-type Cdk5 (Cdk5-WT; Fig. 6*H*,*I*). These data suggest that attractive Ca^{2+} signals suppress clathrin-mediated endocytosis through Cdk5.

Because p35, an activation subunit of Cdk5, interacts with CaMKII in a Ca^{2+}-dependent manner (Dhavan et al., 2002), we hypothesized that CaMKII links attractive Ca^{2+} signals with Cdk5 activation, leading to the suppression of clathrin-mediated endocytosis. As expected, inhibition of CaMKII with KN93 or myr-AIP allowed growth cones to have asymmetric CCP formation in response to attractive Ca^{2+} signals (Fig. 6*F*,*G*). To exclude the possibility that inhibitors of CaMKII and Cdk5 perturbed endocytosis via blocking CICR (i.e., converting attractive Ca^{2+} signals to repulsive ones), we performed Ca^{2+} imaging combined with photolysis of NP-EGTA (for details, see Materials and Methods; Ooashi et al., 2005; Tojima et al., 2009). Inhibition of neither CaMKII nor Cdk5 abolished CICR components of attractive Ca^{2+} signals (Fig. 7), indicating that the generation of CICR is independent of CaMKII and Cdk5 activities. Our data are consistent with the hypothesis that CaMKII and Cdk5 act downstream of attractive Ca^{2+} signals to suppress endocytosis that is otherwise enhanced by these Ca^{2+} signals (Fig. 1*B*).

We further confirmed the involvement of CaMKII in the regulation of endocytosis using CaMKII mutants (Fig. 6*J*–*L*). Ca^{2+}/CaM is necessary for the initial activation of CaMKII, but autophosphorylation at Thr 286 of CaMKII renders the kinase constitutively active independently of Ca^{2+}/CaM (Hudmon and Schulman, 2002). Therefore, we used a Venus-tagged phosphomimetic (constitutively active) mutant of CaMKII, in which Thr was replaced with Asp at 286 (CaMKII-T286D), and a Venus-tagged phospho-deficient mutant of CaMKII as a control, in which Thr was replaced with Ala at 286 (CaMKII-T286A). Repulsive Ca^{2+} signals caused asymmetric CCP formation in growth cones expressing CaMKII-T286A (Fig. 6*J*), but failed to affect CCP formation in growth cones expressing CaMKII-T286D (Fig. 6*K*). These results suggest that, even in the absence of CICR, persistent activation of CaMKII by autophosphorylation is sufficient to suppress Ca^{2+}-induced endocytosis. We then investigated whether CaMKII and Cdk5 act sequentially or in parallel. In growth cones receiving repulsive Ca^{2+} signals, asymmetric CCP formation was suppressed by CaMKII-T286D (Fig. 6*K*), but was rescued after additional treatment with roscovitine (Fig. 6*L*), suggesting that Cdk5 acts downstream of CaMKII.

In presynaptic terminals, PIPKIγ90 interaction with the clathrin adaptor AP-2 is essential for synaptic vesicle endocytosis and this interaction is abolished by a phosphomimetic mutation in

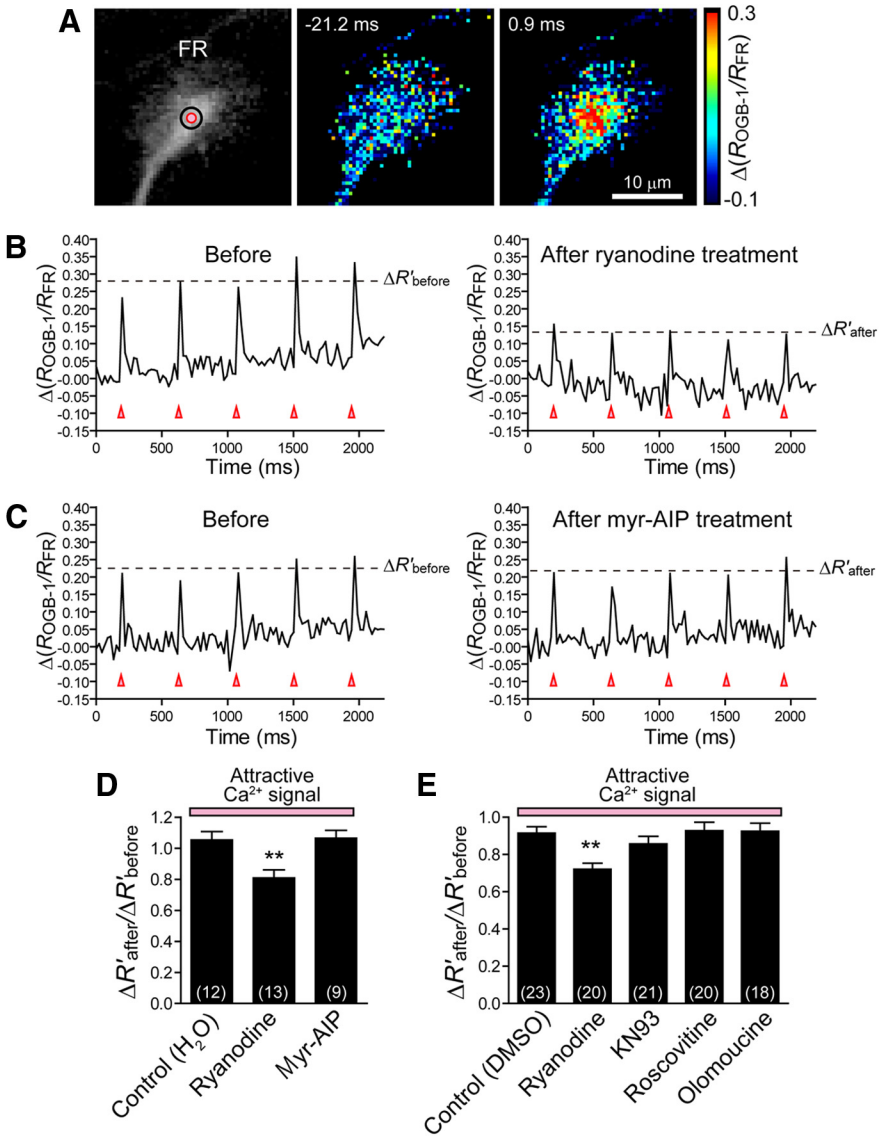

Figure 7. CICR is independent of CaMKII and Cdk5. ***A***, Growth cone loaded with NP-EGTA and two Ca^{2+} indicators, OGB-1 and FR. As Ca^{2+} concentrations elevate, OGB-1 augments and FR attenuates fluorescence emission. In the black-and-white image of FR fluorescence, the pink spot represents the site of laser irradiation and the black circle represents ROI used to quantify Ca^{2+}-signal amplitude. The pseudocolor time-lapse images show changes in the ratio of OGB-1 to FR fluorescence intensities [$\Delta(R_{OGB-1}/R_{FR})$, where $R = F/F_0$], before and after focal laser-induced photolysis. $\Delta(R_{OGB-1}/R_{FR})$ represents relative concentrations of cytosolic Ca^{2+} (for details, see Materials and Methods). Time in milliseconds after a single laser irradiation is shown. Scale bar, 10 μm. ***B***, ***C***, Time course changes in $\Delta(R_{OGB-1}/R_{FR})$ within the ROI before (left) and 5 min after (right) treatment with high-dose ryanodine (***B***) or myr-AIP (***C***). Note that five laser pulses (pink arrowheads) triggered five Ca^{2+} elevations. Before and after the drug treatment, photolysis-induced attractive Ca^{2+} signals were analyzed in the same growth cones under the same experimental conditions. The dashed lines indicate the mean of the five peak $\Delta(R_{OGB-1}/R_{FR})$ values before ($\Delta R'_{before}$) and after ($\Delta R'_{after}$) the drug treatment. ***D***, ***E***, $\Delta R'_{after}/\Delta R'_{before}$ represents drug-induced changes in the amplitude of attractive Ca^{2+} signals. Vehicle only, H_2O (***D***), or DMSO (***E***) was used as a control. The Ca^{2+} signal amplitude decreased after the treatment with high-dose ryanodine, consistent with the fact that attractive Ca^{2+} signals contain CICR. Neither CaMKII inhibitors (KN93 or myr-AIP) nor Cdk5 inhibitors (roscovitine or olomoucine) affected the Ca^{2+} signal amplitude, indicating that CICR generation is independent of CaMKII and Cdk5 activities. Numbers in parentheses indicate the total number of growth cones examined. Error bars represent SEM. $^{**}p < 0.01$ versus control, Dunnett's multiple-comparison test.

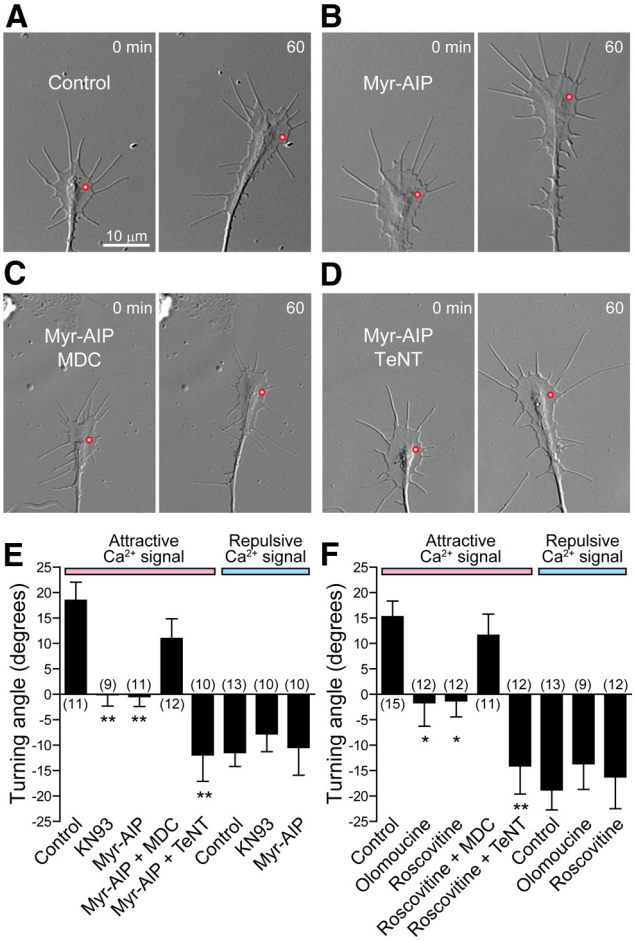

Figure 8. Exocytosis–endocytosis imbalance underlies Ca^{2+}-induced growth cone guidance. ***A–D***, Time-lapse DIC images of growth cones in the absence (control; ***A***) or presence (***B–D***) of the indicated drugs. Attractive Ca^{2+} signals were generated by laser photolysis of NP-EGTA at pink spots. Time in minutes after the onset of repetitive laser irradiation is shown. Scale bar, 10 μm. ***E***, ***F***, Ca^{2+}-induced turning of growth cones in the absence (control) or presence of the indicated drugs. Positive and negative values expressed as mean ± SEM indicate attractive and repulsive turning angles, respectively. Numbers in parentheses indicate the number of growth cones examined. $^*p < 0.05$, $^{**}p < 0.01$ versus control, Dunnett's multiple-comparison test.

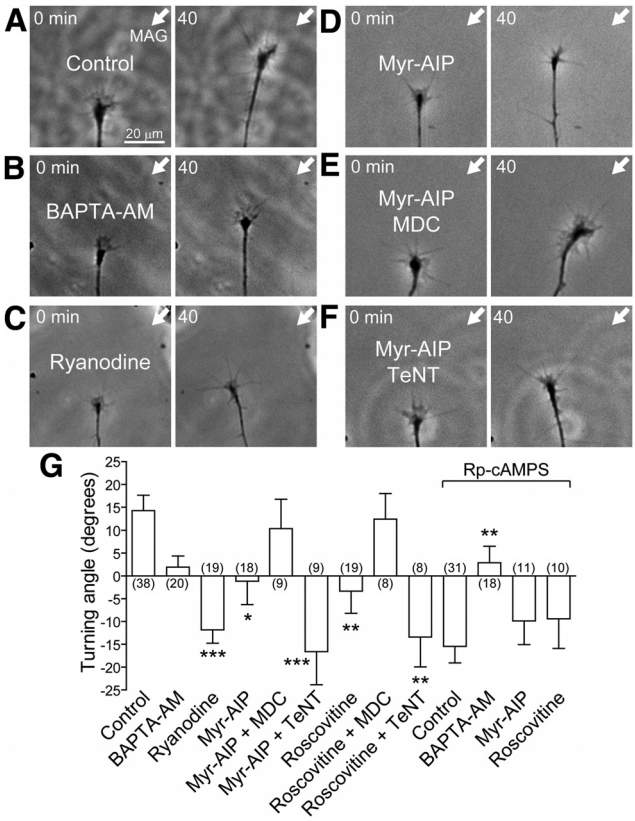

Figure 9. The involvement of CaMKII, Cdk5 and membrane trafficking in MAG-induced growth cone turning. ***A–F***, Time-lapse phase contrast images of growth cones exposed to MAG gradients (arrows) in the absence (control; ***A***) or presence (***B–F***) of the indicated drugs in bath. Time in minutes after the onset of MAG application is shown. Scale bar, 20 μm. ***G***, Growth-cone-turning responses to attractive and repulsive MAG gradients generated in the absence and presence of Rp-cAMPS, respectively. The effects of the indicated drugs were tested. Positive and negative values expressed as mean ± SEM indicate attractive and repulsive turning angles, respectively. Numbers in parentheses indicate the number of growth cones examined. $^*p < 0.05$, $^{**}p < 0.01$, $^{***}p < 0.001$ versus control, Dunnett's multiple-comparison test.

mouse PIPKIγ90 at the Cdk5-phosphorylatable S645 (corresponding to S649 in chicken; Nakano-Kobayashi et al., 2007). To determine whether PIPKIγ90 acts downstream of Cdk5 to suppress endocytosis in growth cones, we transfected DRG neurons with EGFP-tagged chicken PIPKIγ90-WT or its phosphomimetic mutant, in which Ser was replaced with Glu at 649 (PIPKIγ90-S649E; Fig. 6*M–O*). PIPKIγ90-WT transfection had no detectable effect on Ca^{2+}-induced endocytosis: attractive Ca^{2+} signals caused asymmetric CCP formation in roscovitine-treated growth cones (Fig. 6*N*), but not in untreated growth cones (Fig. 6*M*). However, in growth cones expressing PIPKIγ90-S649E, roscovitine treatment failed to allow growth cones to have asymmetric CCP formation in response to attractive Ca^{2+} signals (Fig. 6*O*), consistent with the hypothesis that Cdk5 suppresses endocytosis via PIPKIγ90 phosphorylation at S649. Together, our results show that attractive Ca^{2+} signals, which also involve Ca^{2+} components stimulating endocytosis, can antagonize this inherent repulsive activity via CaMKII and Cdk5 that can inactivate PIPKIγ90 possibly through S649 phosphorylation (Fig. 1*B*).

Exocytosis–endocytosis imbalance underlies Ca^{2+}-induced growth cone guidance

In growth cones receiving attractive Ca^{2+} signals, VAMP2-mediated exocytosis increases (Tojima et al., 2007) but clathrin-mediated endocytosis remains unchanged due to the suppression mediated by CaMKII and Cdk5 (Fig. 6). Therefore, we hypothesized that Ca^{2+} signals induce growth cone turning through localized imbalance between exocytosis and endocytosis. To test this possibility, we quantified Ca^{2+}-induced turning after perturbing the exocytosis–endocytosis imbalance (Fig. 8). Inhibition of CaMKII or Cdk5 with a bath application of relevant drugs caused growth cones to exhibit straight migration even in the presence of attractive Ca^{2+} signals (Fig. 8*B*,*E*,*F*). This is most likely because attractive Ca^{2+} signals under these experimental conditions promoted endocytosis (Fig. 6) that balanced with Ca^{2+}-facilitated exocytosis. Conversely, these inhibitors of CaMKII or Cdk5 did not affect Ca^{2+}-induced repulsion (Fig. 8*E*,*F*). We next investigated whether growth cones can resume turning responses to attractive Ca^{2+} signals after pharmacological treatment that, again, perturbs the balanced activation of exocytosis and endocytosis caused by CaMKII or Cdk5 inhibition. Treatment with MDC, an inhibitor of clathrin-mediated endocytosis, restored attractive turning responses even in the presence of CaMKII or Cdk5 inhibitors (Fig. 8*C*,*E*,*F*). In contrast, treatment

with TeNT, an inhibitor of VAMP2-mediated exocytosis, caused growth cones to exhibit repulsive responses to attractive Ca^{2+} signals in the presence of CaMKII or Cdk5 inhibitors (Fig. 8*D–F*). These results indicate that Ca^{2+} signals on one side of the growth cone can induce bidirectional turning responses via an exocytosis–endocytosis imbalance and that the growth cone turns attractively or repulsively if exocytosis or endocytosis predominates, respectively.

Exocytosis–endocytosis imbalance underlies growth cone guidance mediated by MAG

We next investigated whether a localized imbalance of exocytosis and endocytosis underlies growth cone turning induced by an extracellular concentration gradient of a physiological guidance cue (Figs. 9, 10, 11). Consistent with our previous reports (Tojima et al., 2007; Tojima et al., 2010), directional application of MAG through a glass micropipette attracted or repelled the growth cone in the absence or presence of bath-applied Rp-cAMPS, respectively (Fig. 9*A*,*G*). These bidirectional responses to MAG were negated by pretreating neurons with BAPTA-AM, a fast chelator of cytosolic Ca^{2+} (Fig. 9*B*,*G*). Furthermore, MAG-induced attraction was converted into repulsion when CICR was inhibited with a high dose of ryanodine that traps RyRs in the closed state (Fig. 9*C*,*G*). These results strongly support the idea that Ca^{2+} signals with and without CICR mediate MAG-induced attraction and repulsion, respectively.

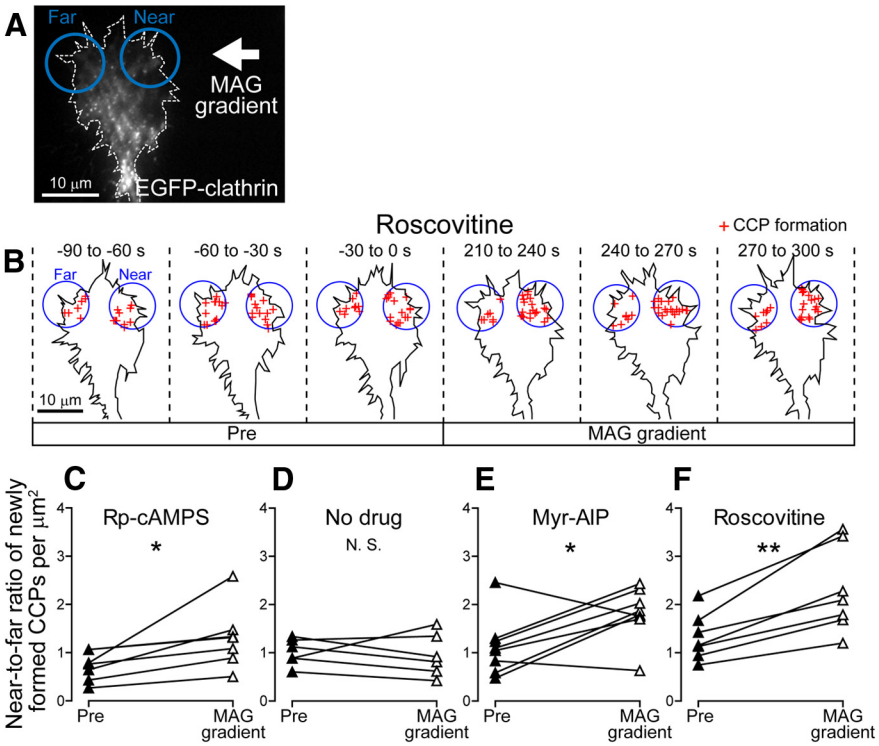

Figure 10. Attractive MAG gradients suppress endocytosis via CaMKII and Cdk5. ***A***, TIRFM image of EGFP-clathrin in a growth cone treated with roscovitine. The growth cone was exposed to an extracellular gradient of MAG (arrow) that acted as an attractive cue in the absence of Rp-cAMPS. The blue circles indicate near and far ROIs for analyses. Scale bar, 10 μm. ***B***, Schematic representation of the growth cone shown in ***A***. TIRFM images of EGFP-clathrin were acquired every 3 s before (pre) and after the onset (time 0 s) of MAG gradient application. Each red cross marks the position of a newly formed CCP within the ROIs during the indicated 30 s periods. Scale bar, 10 μm. ***C–F***, Near-to-far ratios of CCP formation. The *y*-axis indicates the number of newly formed CCPs per unit area within near ROI divided by that within far ROI, before (pre; −120 to 0 s) and after (MAG gradient; 180 to 300 s) the onset of gradient application. Each line represents a MAG-induced change in a single growth cone. MAG gradients were repulsive (***C***) or attractive (***D–F***) in the presence or absence of Rp-cAMPS, respectively. The effects of attractive MAG gradients were determined in the absence (no drug; ***D***) or presence of bath-applied myr-AIP (***E***) or roscovitine (***F***). $*p < 0.05$, $**p < 0.01$; N.S., not significant, paired *t* test.

To determine whether MAG gradients induce asymmetric clathrin-mediated endocytosis across the growth cone, spatiotemporal dynamics of EGFP-clathrin were visualized by TIRFM (Fig. 10). Directional application of MAG in the presence of Rp-cAMPS (repulsive MAG gradients) caused asymmetric formation of CCPs with more CCPs on the side of the growth cone facing the source of MAG (Fig. 10*C*). Conversely, MAG application in the absence of Rp-cAMPS (attractive MAG gradients) had no detectable effect on the relative activity of endocytosis (Fig. 10*D*). These data are consistent with our previous findings that MAG-induced growth cone repulsion, but not attraction, depends on clathrin-meditated endocytosis (Tojima et al., 2010). We then investigated the involvement of CaMKII and Cdk5 in the regulation of endocytosis downstream of attractive MAG signals (Fig. 10*A*,*B*,*E*,*F*). In the presence of myr-AIP or roscovitine, CCP formation became asymmetric in response to attractive MAG gradients, suggesting that attractive MAG suppresses clathrin-mediated endocytosis through CaMKII and Cdk5.

We also investigated whether CaMKII and Cdk5 are involved in MAG-induced exocytosis in growth cones. Because MAG-induced attraction depends on VAMP2-meditated exocytosis (Tojima et al., 2007), we visualized VAMP2-mediated exocytosis in growth cones that expressed a pH-sensitive version of Venus fused to the luminal side of VAMP2 (pHVenus-VAMP2; Tojima et al., 2007; Fig. 11). Attractive MAG gradients induced asymmetric VAMP2-mediated exocytosis, with higher exocytic activity on the near side of the growth cone facing the source of MAG (Fig. 11*F*,*H*,*I*). This asymmetry in exocytosis was not abolished by treatment with myr-AIP or roscovitine (Fig. 11*A–D*,*G–I*), indicating that asymmetric exocytosis for MAG-induced attraction is evoked independently of CaMKII and Cdk5.

Our results so far indicated that, in growth cones with reduced activity of CaMKII or Cdk5, attractive MAG facilitates both exocytosis and endocytosis on their near side (Figs. 10, 11). Therefore, to determine the necessity of exocytosis–endocytosis imbalance, we quantified MAG-induced turning of growth cones treated with inhibitors of CaMKII or Cdk5. In the presence of myr-AIP or roscovitine, growth cones exhibited straight migration in attractive MAG gradients (Fig. 9*D*,*G*), suggesting that the balanced activation of exocytosis and endocytosis impeded attractive turning. Conversely, these drugs did not affect MAG-induced repulsion in the presence of Rp-cAMPS (Fig. 9*G*). We also investigated whether growth cones can resume turning responses to attractive MAG gradients after pharmacological treatment that, again, perturbs the balanced activation of exocytosis and endocytosis caused by CaMKII or Cdk5 inhibition. Treatment with MDC restored MAG-induced attraction even in the presence of myr-AIP or roscovitine (Fig. 9*E*,*G*). In contrast, treatment with TeNT caused growth cones to exhibit repulsive

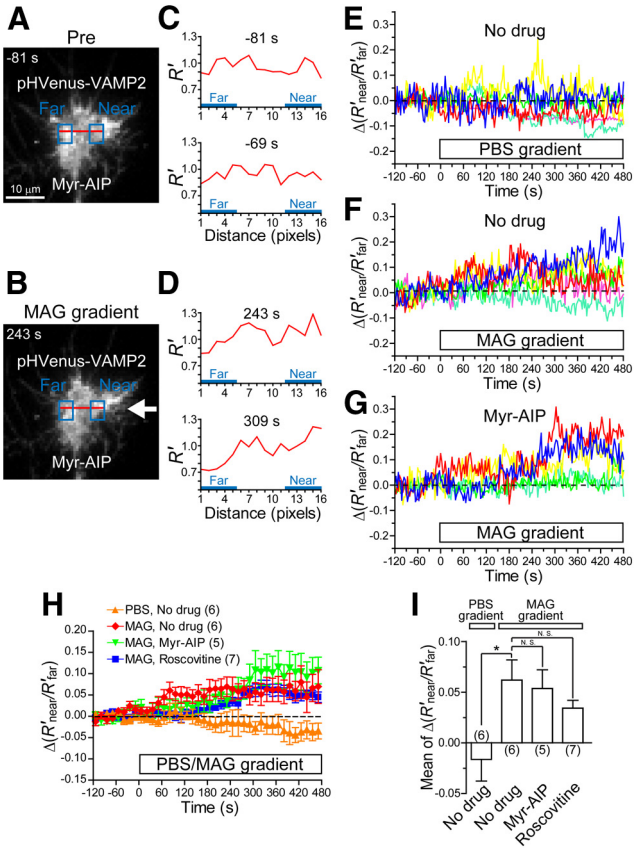

Figure 11. Attractive MAG gradients evoke asymmetric exocytosis independently of CaMKII and Cdk5. ***A***, ***B***, Neurons coexpressing pHVenus-VAMP2 and mCherry-CAAX were cultured in the presence of bath-applied myr-AIP. Shown are pHVenus images of a single growth cone, 81 s before (pre; ***A***) and 243 s after (***B***) the onset of MAG gradient application (arrow in ***B***). The red lines in ***A*** and ***B*** are used for line-scan analyses in ***C*** and ***D***, respectively. The blue rectangles are near and far ROIs for ***E***–***I***. Scale bar, 10 μm. ***C***, ***D***, Line profiles of R', an index of VAMP2 exocytosis, before (***C***) and after (***D***) the onset of MAG gradient application at the indicated time points. R' represents $R_{pHVenus}/R_{mCherry}$, where $R_{pHVenus}$ and $R_{mCherry}$ are F/F_0 values for pHVenus and mCherry, respectively. ***E***–***G***, Superimposed traces of time course of $\Delta(R'_{near}/R'_{far})$, an index of near-to-far asymmetry in VAMP2 exocytosis. $\Delta(R'_{near}/R'_{far}) = R'_{near}/R'_{far} - 1$, where R'_{near} and R'_{far} represent R' values for near and far ROIs, respectively. Each colored line represents $\Delta(R'_{near}/R'_{far})$ in a single growth cone exposed to PBS gradients (***E***) or attractive MAG gradients (***F***,***G***) in the absence (no drug; ***E***,***F***) or presence (***G***) of bath-applied myr-AIP. The *x*-axis represents time in seconds after the onset of PBS or MAG gradient. ***H***, Averaged time course changes in $\Delta(R'_{near}/R'_{far})$ induced by PBS or MAG gradients in the absence (no drug) or presence of bath-applied myr-AIP or roscovitine. Numbers in parentheses indicate the number of growth cones examined. Error bars represent SEM. ***I***, The mean of $\Delta(R'_{near}/R'_{far})$ values during the period from 180 to 297 s after the onset of gradient application. $^*p < 0.05$; N.S., not significant, Bonferroni's multiple-comparison test.

responses to attractive MAG gradients in the presence of myr-AIP or roscovitine (Fig. 9*F*,*G*). These results are consistent with mechanisms underlying Ca^{2+}-induced turning (Fig. 8) and strongly suggest that such Ca^{2+}-dependent regulation of exocytosis–endocytosis imbalance also operates in growth cone guidance induced by physiological cues.

Exocytosis–endocytosis imbalance is necessary for growth cone turning induced by asymmetric membrane perturbation

Finally, we studied growth cone turning induced by direct manipulation of membrane trafficking. Our previous study (Tojima et al., 2010) showed that an extracellular gradient of the endocytosis inhibitor MDC induces asymmetric clathrin-mediated endocytosis across the growth cone and its turning toward the side with less endocytosis. We also reported that a gradient of the exocytosis stimulator α-LTX causes asymmetric VAMP2-mediated exocytosis and growth cone turning toward the side with more exocytosis (Tojima et al., 2010). Consistent with these findings, here, growth cones showed attractive turning toward higher concentrations of MDC (Fig. 12*A*,*D*) or α-LTX (Fig. 12*B*,*D*), confirming that asymmetric endocytosis or exocytosis is sufficient to trigger growth cone turning. We then applied MDC from one side and α-LTX from the other side (Fig. 12*C*,*D*) to create activity gradients of endocytosis and exocytosis of the same

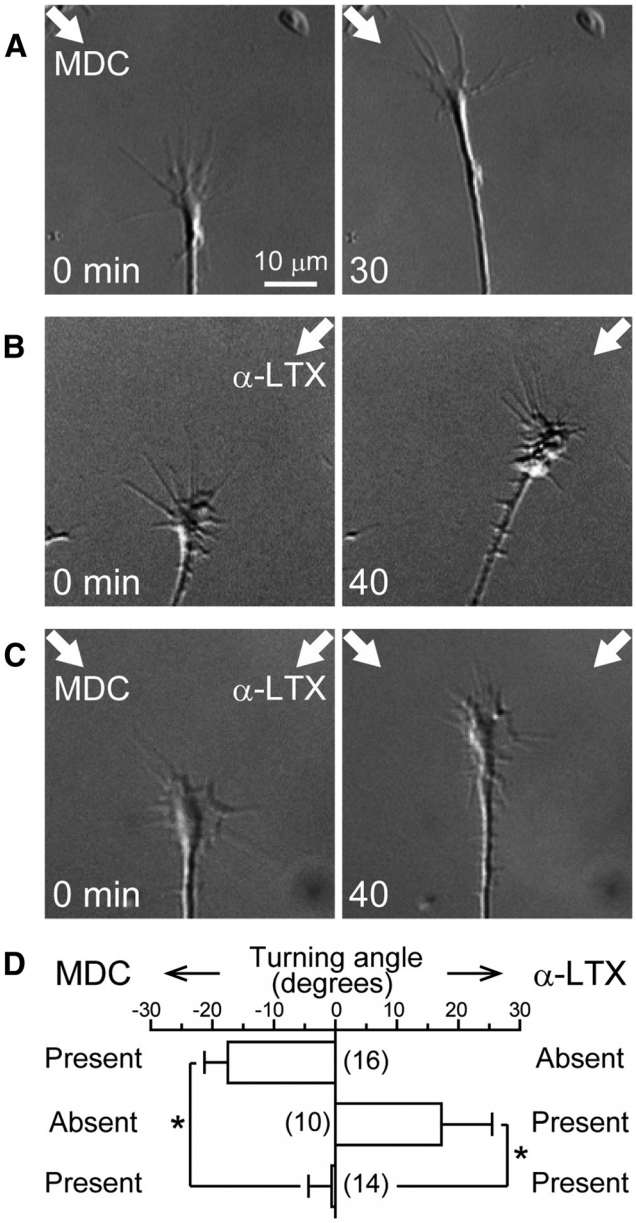

Figure 12. Exocytosis– endocytosis imbalance is necessary for growth cone turning induced by asymmetric membrane perturbation. ***A***–***C***, Time-lapse DIC images of growth cones exposed to gradients of MDC (***A***), α-LTX (***B***),or both simultaneously from opposite sides (***C***) as indicated by the arrows. Time in minutes after the onset of gradient application is shown. Scale bar, 10 μm. ***D***, Growth-cone-turning responses to directionally applied MDC, α-LTX, or both. In case of simultaneous application of two gradients, the sources of MDC and α-LTX were positioned on opposite sides across the growth cone. Positive and negative values expressed as mean $\pm$ SEM indicate turning angles toward α-LTX and MDC gradients, respectively. Numbers in parentheses indicate the number of growth cones examined. $^*p < 0.05$, Bonferroni's multiple-comparison test.

polarity across the growth cone. Such treated growth cones did not exhibit any biased turning (Fig. 12*D*), probably because endocytosis and exocytosis were balanced, consistent with the growth cone's straight migration response to attractive signals after CaMKII or Cdk5 inhibition (Figs. 8, 9).

Discussion

Because axon guidance signals can activate both attractive and repulsive pathways, a growth cone must regulate these signals in a biased manner that forces its steering machinery toward a clear-cut decision between an attractive or repulsive turning response. Here, we have identified Ca^{2+}-dependent signaling pathways that mediate the exocytosis–endocytosis imbalance for growth cone turning (Fig. 1*B*). Because axon guidance also relies on receptor trafficking (O'Donnell et al., 2009), such as endocytosis of Wnt receptors at filopodia tips for Wnt-induced growth cone steering (Onishi et al., 2013), we have investigated membrane-trafficking events downstream of Ca^{2+} signals using direct Ca^{2+} manipulation that can bypass any receptor proximal processes upstream of Ca^{2+}. Our results indicate that, downstream of attractive guidance signals, both VAMP2-mediated exocytosis and clathrin-mediated endocytosis are regulated differentially such that exocytosis predominates over endocytosis to ensure attractive turning. This regulation involves suppression of endocytosis by CaMKII and Cdk5 that potentially catalyzes phosphorylation and inactivation of PIPKIγ90. In contrast, repulsive guidance signals selectively facilitate endocytosis for repulsive turning (Tojima et al., 2010). Most importantly, we have demonstrated in the present study that growth cone turning requires an exocytosis–endocytosis imbalance and that the turning direction is determined by the relative predominance between these opposing membrane-trafficking events (Fig. 13).

This study, along with previous reports (Wen et al., 2004; Tojima et al., 2010), suggests that repulsive Ca^{2+} signals selectively activate only calcineurin, whereas attractive Ca^{2+} signals activate both CaMKII and calcineurin. How can Ca^{2+} activate these two effectors differentially? It is thought that the amplitude of attractive Ca^{2+} signals is higher than that of repulsive Ca^{2+} signals (Henley et al., 2004; Nishiyama et al., 2008) because attractive Ca^{2+} signals are the sum of repulsive Ca^{2+} signals and CICR (Ooashi et al., 2005). Therefore, one plausible explanation is that the difference in Ca^{2+} signal amplitude is responsible for the selective activation of downstream effectors. Indeed, CaMKII and calcineurin have different affinity for Ca^{2+}/CaM: calcineurin has a higher affinity for Ca^{2+}/CaM than CaMKII (Rusnak and Mertz, 2000; Hudmon and Schulman, 2002). Dual imaging of CaMKII and calcineurin activities in single dendritic spines has provided consistent results with this Ca^{2+} affinity model: smaller Ca^{2+} elevations activate calcineurin but not CaMKII, whereas larger Ca^{2+} elevations activate both calcineurin and CaMKII (Fujii et al., 2013). The source of Ca^{2+} signals is another determinant of effector activation, because Ca^{2+} signals of equivalent amplitude with or without CICR cause growth cone attraction or repulsion, respectively (Ooashi et al., 2005). In this Ca^{2+} source model, CaMKII located in close proximity to RyRs (Zalk et al., 2007) may be activated specifically by CICR. Probably, both the amplitude and the source of Ca^{2+} signals influence cytoplasmic Ca^{2+} concentrations on the ER, thereby activating distinct sets of downstream effectors.

Our results also raise the possibility that Ca^{2+}-activated CaMKII then translocates toward the plasma membrane and regulates Cdk5 to suppress clathrin-mediated endocytosis. The Cdk5 activator p35 is highly phosphorylated by CaMKII in embryonic brain (Hosokawa et al., 2010). Furthermore, glutamate stimulation of hippocampal neurons *in vitro* enhances CaMKII interactions with p35 in a Ca^{2+}-dependent manner, but does not alter the kinase activity of Cdk5 (Dhavan et al., 2002). These findings are consistent with the hypothesis that, although CaMKII may not regulate the Cdk5 kinase activity directly, Ca^{2+}-activated CaMKII could recruit p35 and Cdk5 to relevant areas of the plasma membrane, where Cdk5 could suppress clathrin-mediated endocytosis.

Cdk5 can phosphorylate, not only PIPKIγ90, but also other dephosphins, including dynamin 1, amphyphysin 1, and synap-

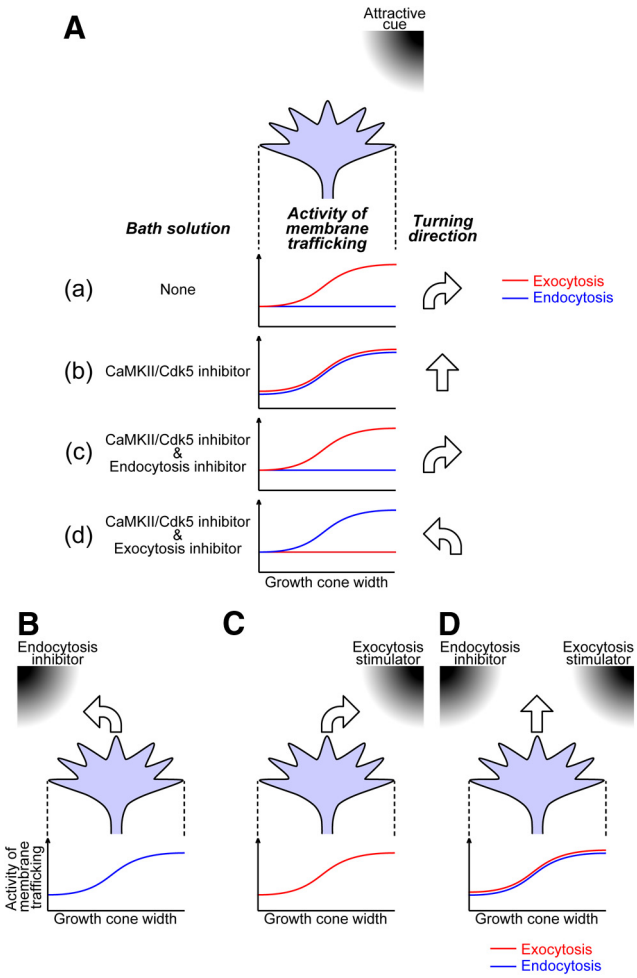

Figure 13. Exocytosis–endocytosis imbalance underlies bidirectional growth cone steering. ***A***, Spatial profiles of membrane-trafficking activities across the growth cone width and turning responses to an extracellular attractive cue. ***Aa***, Normally, exocytosis (red line) predominates on the side facing an attractive cue, whereas endocytosis (blue line) remains symmetric. Such localized predominance of exocytosis over endocytosis drives attractive turning toward the cue. ***Ab***, In the presence of bath-applied CaMKII or Cdk5 inhibitor, an attractive cue activates both exocytosis and endocytosis on the near side of the growth cone. Such asymmetric but balanced facilitation of exocytosis and endocytosis causes straight migration. ***Ac***, Additional treatment with an endocytosis inhibitor reconverts the balanced membrane trafficking into exocytosis predominance and restores the growth cone attractive response to the cue. ***Ad***, Pharmacological suppression of exocytosis in addition to CaMKII or Cdk5 inhibition causes endocytosis predominance and repulsive turning even if the cue is attractive. ***B***–***D***, Direct manipulation of membrane trafficking is sufficient for growth cone turning if exocytosis and endocytosis are not balanced. Extracellular gradients of an endocytosis inhibitor (***B***) and an exocytosis stimulator (***C***) induce growth cone turning toward the side with less endocytosis and more exocytosis, respectively. However, simultaneous application of both gradients most likely creates activity gradients of endocytosis and exocytosis of the same polarity across the growth cone, resulting in its straight migration (***D***).

tojanin 1. Tomizawa et al. (2003) reported that Cdk5-mediated phosphorylation of amphiphysin 1 and dynamin 1 inhibits clathrin-mediated synaptic vesicle endocytosis. Furthermore, the inositol 5-phosphatase synaptojanin 1, which is implicated in synaptic vesicle endocytosis, can be regulated antagonistically by Cdk5 and calcineurin: phosphorylation and dephosphorylation of synaptojanin 1 stimulate and inhibit its phosphatase activity, respectively (Lee et al., 2004). Similar mechanisms may also operate in growth cone guidance, because dephosphins colocalize with p35 in growth cones (Mundigl et al., 1998; Floyd et al., 2001) and participate in repulsive turning (Kolpak et al., 2009; Tojima et al., 2010).

The straight migration of a growth cone, which has simultaneous activation of endocytosis and exocytosis on one side, illustrates their antagonistic effects on growth cone turning. This raises the possibility that endocytic and exocytic membrane vesicles carry functionally similar cargo molecules such as cell adhesion molecules (CAMs). Accumulating evidence indicates that spatially polarized endocytosis and exocytosis of CAMs in growth cones drive axon elongation. For example, a growth cone migrates forward by internalizing L1, an Ig superfamily CAM, via CCPs at the central domain and recycling the endocytosed L1 into the leading edge plasma membrane via exocytosis (Kamiguchi and Lemmon, 2000; Kamiguchi and Yoshihara, 2001; Alberts et al., 2006). Similarly, endocytic recycling of β1-integrin in growth cones drives axon elongation (Eva et al., 2012). It is also possible that such CAM trafficking drives growth cone turning if endocytosis and exocytosis of CAMs are differentially polarized across the growth cone. In agreement with this idea, MAG-induced growth cone repulsion involves asymmetric retrieval of cell-surface β1-integrin via clathrin-mediated endocytosis (Hines et al., 2010). In non-neuronal cells, endocytosed β1-integrin is also present in VAMP2-positive vesicles and depletion of VAMP2 reduces the amount of β1-integrin on the cell surface, which inhibits cell adhesion and chemotactic migration (Hasan and Hu, 2010). These findings support the idea that β1-integrin undergoes clathrin-mediated endocytosis or VAMP2-mediated exocytosis for growth cone turning. In addition to CAMs, cytoskeletal components and their regulatory proteins can be cargoes on intracellular vesicles. Proteomic analyses have identified proteins such as actin, tubulin, Arp2/3, and Rac that associate with VAMP2-positive synaptic vesicles and clathrin-coated vesicles isolated from brain (Blondeau et al., 2004; Takamori et al., 2006). In non-neuronal cells, Rac is attached onto the surface of endosomal vesicles and transported to the cell periphery, where it regulates actin dynamics for cell motility (Palamidessi et al., 2008). These findings suggest an instructive role of the membrane-trafficking system in polarized targeting of cytoskeletal and adhesion components for bidirectional growth cone guidance.

In conclusion, we have demonstrated the antagonistic actions of exocytosis and endocytosis in axon guidance: localized imbalance between these membrane-trafficking events drives growth cone turning toward the side with predominant exocytosis or away from the side with predominant endocytosis. These discoveries provide significant mechanistic insight into polarized cell migration and will contribute to technological innovation for guiding axons to their appropriate targets during nervous system development and regeneration.

References

Akiyama H, Matsu-ura T, Mikoshiba K, Kamiguchi H (2009) Control of neuronal growth cone navigation by asymmetric inositol 1,4,5-trisphosphate signals. Sci Signal 2:ra34. CrossRef Medline

Alberts P, Rudge R, Irinopoulou T, Danglot L, Gauthier-Rouvière C, Galli T (2006) Cdc42 and actin control polarized expression of TI-VAMP vesicles to neuronal growth cones and their fusion with the plasma membrane. Mol Biol Cell 17:1194–1203. CrossRef Medline

Blondeau F, Ritter B, Allaire PD, Wasiak S, Girard M, Hussain NK, Angers A, Legendre-Guillemin V, Roy L, Boismenu D, Kearney RE, Bell AW, Bergeron JJ, McPherson PS (2004) Tandem MS analysis of brain clathrin-coated vesicles reveals their critical involvement in synaptic vesicle recycling. Proc Natl Acad Sci U S A 101:3833–3838. CrossRef Medline

Cousin MA, Robinson PJ (2001) The dephosphins: dephosphorylation by calcineurin triggers synaptic vesicle endocytosis. Trends Neurosci 24: 659–665. CrossRef Medline

Dhavan R, Greer PL, Morabito MA, Orlando LR, Tsai LH (2002) The cyclin-dependent kinase 5 activators p35 and p39 interact with the α-subunit of Ca^{2+}/calmodulin-dependent protein kinase II and α-actinin-1 in a calcium-dependent manner. J Neurosci 22:7879–7891. Medline

Di Paolo G, Pellegrini L, Letinic K, Cestra G, Zoncu R, Voronov S, Chang S, Guo J, Wenk MR, De Camilli P (2002) Recruitment and regulation of phosphatidylinositol phosphate kinase type 1 γ by the FERM domain of talin. Nature 420:85–89. CrossRef Medline

Endo M, Ohashi K, Mizuno K (2007) LIM kinase and slingshot are critical for neurite extension. J Biol Chem 282:13692–13702. CrossRef Medline

Eva R, Crisp S, Marland JR, Norman JC, Kanamarlapudi V, ffrench-Constant C, Fawcett JW (2012) ARF6 directs axon transport and traffic of integrins and regulates axon growth in adult DRG neurons. J Neurosci 32: 10352–10364. CrossRef Medline

Floyd SR, Porro EB, Slepnev VI, Ochoa GC, Tsai LH, De Camilli P (2001) Amphiphysin 1 binds the cyclin-dependent kinase (cdk) 5 regulatory subunit p35 and is phosphorylated by cdk5 and cdc2. J Biol Chem 276:8104–8110. CrossRef Medline

Fujii H, Inoue M, Okuno H, Sano Y, Takemoto-Kimura S, Kitamura K, Kano M, Bito H (2013) Nonlinear decoding and asymmetric representation of neuronal input information by CaMKIIα and calcineurin. Cell Rep 3:978–987. CrossRef Medline

Funakoshi Y, Hasegawa H, Kanaho Y (2011) Regulation of PIP5K activity by Arf6 and its physiological significance. J Cell Physiol 226:888–895. CrossRef Medline

Gaidarov I, Santini F, Warren RA, Keen JH (1999) Spatial control of coated-pit dynamics in living cells. Nat Cell Biol 1:1–7. CrossRef Medline

Gomez TM, Zheng JQ (2006) The molecular basis for calcium-dependent axon pathfinding. Nat Rev Neurosci 7:115–125. CrossRef Medline

Hasan N, Hu C (2010) Vesicle-associated membrane protein 2 mediates trafficking of $\alpha5\beta1$ integrin to the plasma membrane. Exp Cell Res 316: 12–23. CrossRef Medline

Henley JR, Huang KH, Wang D, Poo MM (2004) Calcium mediates bidirectional growth cone turning induced by myelin-associated glycoprotein. Neuron 44:909–916. CrossRef Medline

Hines JH, Abu-Rub M, Henley JR (2010) Asymmetric endocytosis and remodeling of β1-integrin adhesions during growth cone chemorepulsion by MAG. Nat Neurosci 13:829–837. CrossRef Medline

Hong K, Nishiyama M, Henley J, Tessier-Lavigne M, Poo M (2000) Calcium signalling in the guidance of nerve growth by netrin-1. Nature 403:93–98. CrossRef Medline

Hosokawa T, Saito T, Asada A, Fukunaga K, Hisanaga S (2010) Quantitative measurement of in vivo phosphorylation states of Cdk5 activator p35 by Phos-tag SDS-PAGE. Mol Cell Proteomics 9:1133–1143. CrossRef Medline

Hudmon A, Schulman H (2002) Neuronal Ca^{2+}/calmodulin-dependent protein kinase II: the role of structure and autoregulation in cellular function. Annu Rev Biochem 71:473–510. CrossRef Medline

Ishihara H, Shibasaki Y, Kizuki N, Wada T, Yazaki Y, Asano T, Oka Y (1998) Type I phosphatidylinositol-4-phosphate 5-kinases: cloning of the third isoform and deletion/substitution analysis of members of this novel lipid kinase family. J Biol Chem 273:8741–8748. Medline

Kamiguchi H, Lemmon V (2000) Recycling of the cell adhesion molecule L1 in axonal growth cones. J Neurosci 20:3676–3686. Medline

Kamiguchi H, Yoshihara F (2001) The role of endocytic L1 trafficking in polarized adhesion and migration of nerve growth cones. J Neurosci 21: 9194–9203. Medline

Kolpak AL, Jiang J, Guo D, Standley C, Bellve K, Fogarty K, Bao ZZ (2009) Negative guidance factor-induced macropinocytosis in the growth cone

plays a critical role in repulsive axon turning. J Neurosci 29:10488–10498. CrossRef Medline

Kurokawa K, Mochizuki N, Ohba Y, Mizuno H, Miyawaki A, Matsuda M (2001) A pair of fluorescent resonance energy transfer-based probes for tyrosine phosphorylation of the CrkII adaptor protein in vivo. J Biol Chem 276:31305–31310. CrossRef Medline

Lee SY, Wenk MR, Kim Y, Nairn AC, De Camilli P (2004) Regulation of synaptojanin 1 by cyclin-dependent kinase 5 at synapses. Proc Natl Acad Sci U S A 101:546–551. CrossRef Medline

Lee SY, Voronov S, Letinic K, Nairn AC, Di Paolo G, De Camilli P (2005) Regulation of the interaction between PIPKIγ and talin by proline-directed protein kinases. J Cell Biol 168:789–799. CrossRef Medline

Ling K, Doughman RL, Firestone AJ, Bunce MW, Anderson RA (2002) Type I γ phosphatidylinositol phosphate kinase targets and regulates focal adhesions. Nature 420:89–93. CrossRef Medline

Loijens JC, Anderson RA (1996) Type I phosphatidylinositol-4-phosphate 5-kinases are distinct members of this novel lipid kinase family. J Biol Chem 271:32937–32943. Medline

Merrifield CJ, Feldman ME, Wan L, Almers W (2002) Imaging actin and dynamin recruitment during invagination of single clathrin-coated pits. Nat Cell Biol 4:691–698. CrossRef Medline

Mundigl O, Ochoa GC, David C, Slepnev VI, Kabanov A, De Camilli P (1998) Amphiphysin I antisense oligonucleotides inhibit neurite outgrowth in cultured hippocampal neurons. J Neurosci 18:93–103. Medline

Nakano-Kobayashi A, Yamazaki M, Unoki T, Hongu T, Murata C, Taguchi R, Katada T, Frohman MA, Yokozeki T, Kanaho Y (2007) Role of activation of PIP5Kγ661 by AP-2 complex in synaptic vesicle endocytosis. EMBO J 26:1105–1116. CrossRef Medline

Nguyen C, Bibb JA (2003) Cdk5 and the mystery of synaptic vesicle endocytosis. J Cell Biol 163:697–699. CrossRef Medline

Nikolic M, Dudek H, Kwon YT, Ramos YF, Tsai LH (1996) The cdk5/p35 kinase is essential for neurite outgrowth during neuronal differentiation. Genes Dev 10:816–825. CrossRef Medline

Nishimura K, Yoshihara F, Tojima T, Ooashi N, Yoon W, Mikoshiba K, Bennett V, Kamiguchi H (2003) L1-dependent neuritogenesis involves ankyrinB that mediates L1-CAM coupling with retrograde actin flow. J Cell Biol 163:1077–1088. CrossRef Medline

Nishiyama M, von Schimmelmann MJ, Togashi K, Findley WM, Hong K (2008) Membrane potential shifts caused by diffusible guidance signals direct growth-cone turning. Nat Neurosci 11:762–771. CrossRef Medline

O'Donnell M, Chance RK, Bashaw GJ (2009) Axon growth and guidance: receptor regulation and signal transduction. Annu Rev Neurosci 32:383–412. CrossRef Medline

Onishi K, Shafer B, Lo C, Tissir F, Goffinet AM, Zou Y (2013) Antagonistic functions of Dishevelleds regulate Frizzled3 endocytosis via filopodia tips in Wnt-mediated growth cone guidance. J Neurosci 33:19071–19085. CrossRef Medline

Ooashi N, Futatsugi A, Yoshihara F, Mikoshiba K, Kamiguchi H (2005) Cell adhesion molecules regulate Ca^{2+}-mediated steering of growth cones via cyclic AMP and ryanodine receptor type 3. J Cell Biol 170:1159–1167. CrossRef Medline

Palamidessi A, Frittoli E, Garré M, Faretta M, Mione M, Testa I, Diaspro A, Lanzetti L, Scita G, Di Fiore PP (2008) Endocytic trafficking of Rac is required for the spatial restriction of signaling in cell migration. Cell 134:135–147. CrossRef Medline

Rappoport JZ, Simon SM (2003) Real-time analysis of clathrin-mediated endocytosis during cell migration. J Cell Sci 116:847–855. CrossRef Medline

Rusnak F, Mertz P (2000) Calcineurin: form and function. Physiol Rev 80:1483–1521. Medline

Sasaki T, Takasuga S, Sasaki J, Kofuji S, Eguchi S, Yamazaki M, Suzuki A (2009) Mammalian phosphoinositide kinases and phosphatases. Prog Lipid Res 48:307–343. CrossRef Medline

Takamori S, Holt M, Stenius K, Lemke EA, Grønborg M, Riedel D, Urlaub H, Schenck S, Brügger B, Ringler P, Müller SA, Rammner B, Gräter F, Hub JS, De Groot BL, Mieskes G, Moriyama Y, Klingauf J, Grubmüller H, Heuser J, et al. (2006) Molecular anatomy of a trafficking organelle. Cell 127:831–846. CrossRef Medline

Tan TC, Valova VA, Malladi CS, Graham ME, Berven LA, Jupp OJ, Hansra G, McClure SJ, Sarcevic B, Boadle RA, Larsen MR, Cousin MA, Robinson PJ (2003) Cdk5 is essential for synaptic vesicle endocytosis. Nat Cell Biol 5:701–710. CrossRef Medline

Tessier-Lavigne M, Goodman CS (1996) The molecular biology of axon guidance. Science 274:1123–1133. CrossRef Medline

Tojima T, Akiyama H, Itofusa R, Li Y, Katayama H, Miyawaki A, Kamiguchi H (2007) Attractive axon guidance involves asymmetric membrane transport and exocytosis in the growth cone. Nat Neurosci 10:58–66. CrossRef Medline

Tojima T, Itofusa R, Kamiguchi H (2009) The nitric oxide-cGMP pathway controls the directional polarity of growth cone guidance via modulating cytosolic Ca^{2+} signals. J Neurosci 29:7886–7897. CrossRef Medline

Tojima T, Itofusa R, Kamiguchi H (2010) Asymmetric clathrin-mediated endocytosis drives repulsive growth cone guidance. Neuron 66:370–377. CrossRef Medline

Tojima T, Hines JH, Henley JR, Kamiguchi H (2011) Second messengers and membrane trafficking direct and organize growth cone steering. Nat Rev Neurosci 12:191–203. CrossRef Medline

Tomizawa K, Sunada S, Lu YF, Oda Y, Kinuta M, Ohshima T, Saito T, Wei FY, Matsushita M, Li ST, Tsutsui K, Hisanaga S, Mikoshiba K, Takei K, Matsui H (2003) Cophosphorylation of amphiphysin I and dynamin I by Cdk5 regulates clathrin-mediated endocytosis of synaptic vesicles. J Cell Biol 163:813–824. CrossRef Medline

Unoki T, Matsuda S, Kakegawa W, Van NT, Kohda K, Suzuki A, Funakoshi Y, Hasegawa H, Yuzaki M, Kanaho Y (2012) NMDA receptor-mediated PIP5K activation to produce $PI(4,5)P_2$ is essential for AMPA receptor endocytosis during LTD. Neuron 73:135–148. CrossRef Medline

Wen Z, Guirland C, Ming GL, Zheng JQ (2004) A CaMKII/calcineurin switch controls the direction of Ca^{2+}-dependent growth cone guidance. Neuron 43:835–846. CrossRef Medline

Wenk MR, Pellegrini L, Klenchin VA, Di Paolo G, Chang S, Daniell L, Arioka M, Martin TF, De Camilli P (2001) PIP kinase Iγ is the major $PI(4,5)P_2$ synthesizing enzyme at the synapse. Neuron 32:79–88. CrossRef Medline

Zalk R, Lehnart SE, Marks AR (2007) Modulation of the ryanodine receptor and intracellular calcium. Annu Rev Biochem 76:367–385. CrossRef Medline